THE AUDITORY SYSTEM AND HUMAN SOUND-LOCALIZATION BEHAVIOR

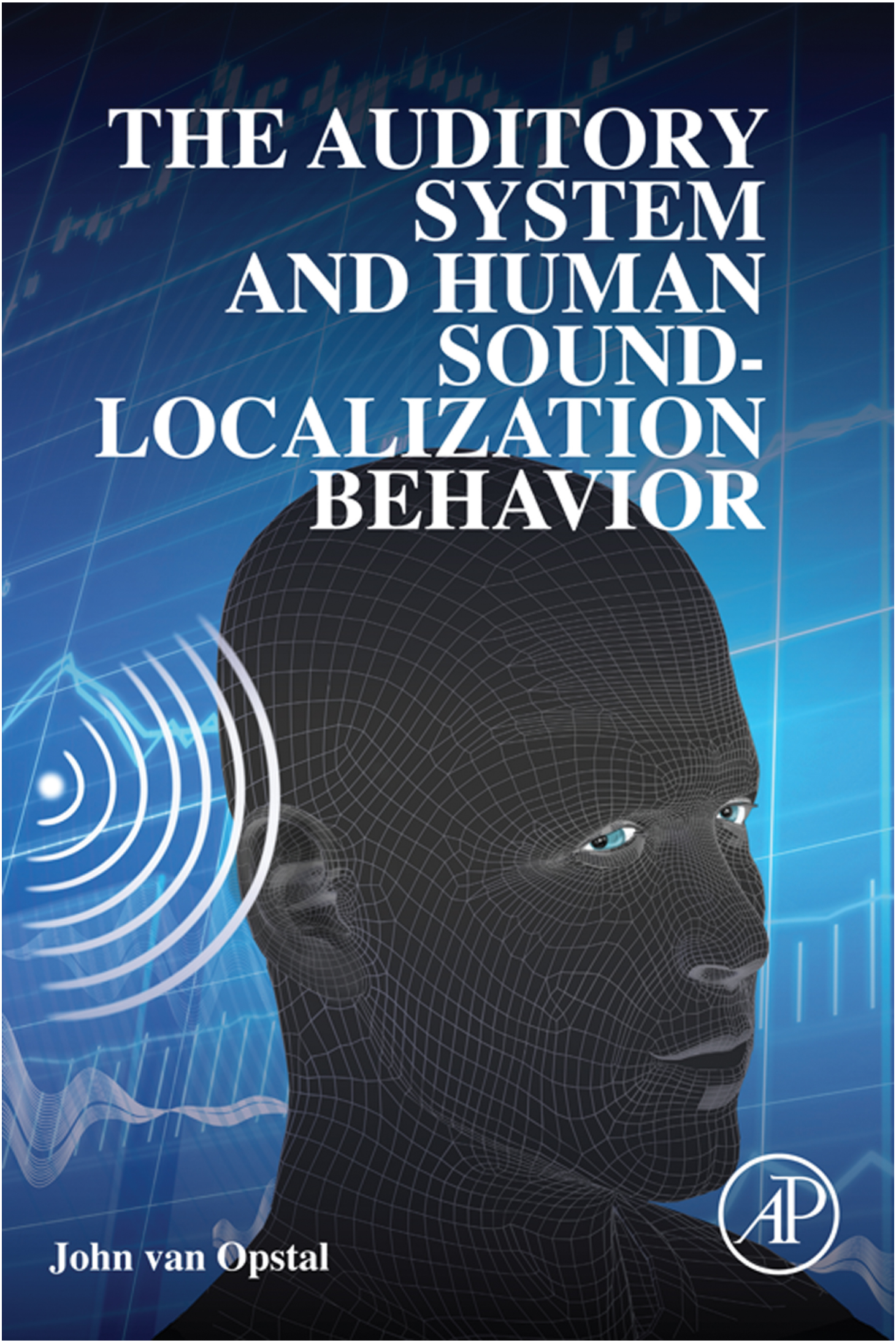

John van Opstal

The Auditory System and Human Sound-Localization Behavior

Page left intentionally blank

The Auditory System and Human Sound-Localization Behavior

John van Opstal
Department of Biophysics
Donders Centre for Neuroscience
Radboud University Nijmegen
The Netherlands

AMSTERDAM • BOSTON • HEIDELBERG • LONDON
NEW YORK • OXFORD • PARIS • SAN DIEGO
SAN FRANCISCO • SINGAPORE • SYDNEY • TOKYO
Academic Press is an Imprint of Elsevier

Academic Press is an imprint of Elsevier
125 London Wall, London EC2Y 5AS, UK
525 B Street, Suite 1800, San Diego, CA 92101-4495, USA
50 Hampshire Street, 5th Floor, Cambridge, MA 02139, USA
The Boulevard, Langford Lane, Kidlington, Oxford OX5 1GB, UK

Notices

Knowledge and best practice in this field are constantly changing. As new research and experience broaden our understanding, changes in research methods, professional practices, or medical treatment may become necessary.

Practitioners and researchers must always rely on their own experience and knowledge in evaluating and using any information, methods, compounds, or experiments described herein. In using such information or methods they should be mindful of their own safety and the safety of others, including parties for whom they have a professional responsibility.

To the fullest extent of the law, neither the Publisher nor the authors, contributors, or editors, assume any liability for any injury and/or damage to persons or property as a matter of products liability, negligence or otherwise, or from any use or operation of any methods, products, instructions, or ideas contained in the material herein.

British Library Cataloguing-in-Publication Data
A catalogue record for this book is available from the British Library

Library of Congress Cataloging-in-Publication Data
A catalog record for this book is available from the Library of Congress

ISBN: 978-0-12-801529-2

Typeset by Thomson Digital
Printed and bound in USA

Dedication

To Dr Dick Donker (Dec 21, 1934–Oct 1, 2014):
neurologist, life artist, lover of music,
and of auditory science.

Page left intentionally blank

Contents

List of Abbreviations xi

1. A Brief Introduction to the Topic
   - 1.1 Two Tasks for the Auditory System 1
   - 1.2 An Ill-Posed Problem 2
   - 1.3 Dealing With Ill-Posed Problems 5
   - 1.4 Spectral Representation and Source Priors 6
   - 1.5 Top–Down Selective Filtering 8
   - 1.6 Audiovisual Integration 11
   - 1.7 How to Use This Book 12
   - 1.8 Overview 15
   - 1.9 Exercises 19
   - Acknowledgment 21
   - References 21

2. The Nature of Sound
   - 2.1 Longitudinal Pressure Waves in a Medium 23
   - 2.2 The Homogeneous Wave Equation 28
     - 2.2.1 Example: Interference and Binaural Beats 31
   - 2.3 Harmonic Sound Waves and Acoustic Impedance 34
   - 2.4 Acoustic Energy, Intensity, Decibel 37
   - 2.5 Reflection, Transmission, and Impedance Matching 38
   - 2.6 Sound Spectrum, Fourier Series, and Bandwidth 42
   - 2.7 Phase Velocity and Group Velocity 46
   - 2.8 Exercises 47
   - References 50

3. Linear Systems
   - 3.1 Modeling Physical and Biological Systems 51
   - 3.2 Linear Systems: The Impulse Response 56
   - 3.3 Linear Systems: The Transfer Characteristic 62
   - 3.4 Combining Linear Systems in Control Schemes 66
   - 3.5 Examples 68
   - 3.6 Linear Systems: The Laplace Transform 71

3.7 Correlation Functions and Gaussian White Noise 79
3.8 Exercises 81
References 86

4. Nonlinear Systems
4.1 Nonlinear Systems Identification 87
4.2 Nonlinear Systems Analysis: The Volterra Series 91
4.3 Nonlinear Systems Analysis: The Wiener Series 93
4.4 Independent Calculation of Volterra Kernels 106
4.5 Exercises 110
References 112

5. The Cochlea
5.1 Introduction: From Acoustic Input to Traveling Wave 113
5.2 Basic Physics Underlying Water Waves 118
5.3 The Linear Cochlear Model (Von Békesy and Zwislocki) 124
5.4 The Active, Nonlinear Cochlea: Role of Outer Hair Cells 134
5.5 Exercises 142
References 145

6. The Auditory Nerve
6.1 Introduction: Tuning of Auditory Nerve Fibers 147
6.2 Reverse Correlation and the Gammatone Filter 148
6.3 Phase Locking 152
6.4 Rate-Level Tuning of the Auditory Nerve 156
6.5 Two-Tone Suppression 158
6.6 Modeling the Auditory Nerve 159
6.7 Multitone Responses of the Auditory Nerve 163
6.8 Exercises 168
References 168

7. Acoustic Localization Cues
7.1 Introduction 171
7.2 Interaural Time Differences 173
7.2.1 Jeffress' Delay-Line Model 176
7.2.2 Modeling Coincidence Detection 179
7.2.3 Timed Inhibition 180
7.2.4 Timed Inhibition? 183
7.3 Interaural Level Differences 184
7.3.1 ILD Encoding at the LSO 187
7.4 The Cone of Confusion 188
7.5 Spectral Pinna Cues 190
7.5.1 Possible Neural Correlate for Spectral Cues 194
7.5.2 Localization in Elevation: An Ill-Posed Problem 195
7.5.3 Alternative Elevation Cues? 199

7.6 Distance Perception 201
7.6.1 The Free Far Field 201
7.6.2 The Free Near Field 202
7.6.3 Reverberant Environments 203
7.7 Exercises 205
References 206

8. Assessing Auditory Spatial Performance
8.1 Introduction 209
8.2 Signal-Detection Theory 210
8.3 Detection, Lateralization, Discrimination, and Localization 218
8.4 Sound Localization: Prey Versus Predator 228
8.5 Sound Localization: Effects of Spectral Content, Duration, and Level 230
8.5.1 Binaural Spectral Weighting 236
8.6 Virtual Acoustics 240
8.7 Exercises 242
References 243

9. The Gaze-Orienting System
9.1 Introduction 245
9.2 Saccadic Eye Movements 248
9.3 Saccadic Eye–Head Gaze Shifts 262
9.4 Auditory and Visual-Evoked Gaze Saccades 265
9.5 Exercises 269
References 271

10. The Midbrain Colliculus
10.1 Introduction 273
10.2 A Multisensory Motor Map for Gaze Orienting 278
10.3 SC: A Vectorial Pulse Generator 285
10.4 IC: Putative Role in Spatial Hearing 296
10.5 Exercises 301
References 303

11. Coordinate Transformations
11.1 Introduction 305
11.2 Gain Fields and Predictive Remapping 310
11.3 The Static Double-Step Paradigm 313
11.3.1 Eye–Head Coordination 315
11.4 Dynamic Double Step: Visual and Auditory 317
11.5 Spatial Hearing is Influenced by Eye- and Head Position 323
11.6 Limits to Updating? 325
11.7 Exercises 330
References 330

12. Sound Localization Plasticity
12.1 Introduction 333
12.2 Learning Binaural Cues 341
12.3 Learning Spectral Cues 345
12.4 Visual Factors in Learning 351
12.5 Limits to Plasticity? 356
12.6 Exercises 358
References 358

13. Multisensory Integration
13.1 Introduction 361
13.2 Models 368
13.3 Bayesian Inference 371
13.4 AV Congruent 380
13.5 AV Incongruent 383
13.6 Audio-Vestibular Integration 387
13.7 Exercises 390
References 390

14. Impaired Hearing and Sound Localization
14.1 Introduction 393
14.2 Restorative Hearing Technologies 397
14.3 Single-Sided Deafness 399
14.4 Unilateral Conductive Hearing Loss 404
14.5 Bimodal Hearing: CI–HA 407
14.6 Presbycusis: Sometimes Superior Performance? 409
References 411

Subject Index 413

List of Abbreviations

2AFC	Two-alternative forced choice
AC	Auditory cortex
AM	Amplitude modulation
AMP	Auditory median plane
AN	Auditory nerve
ANN	Artificial neural network
AV	Audiovisual
AVCN	Antero-ventral part of Cochlear Nucleus
BB	Black box
BCD	Bone-conduction device
BM	Basilar membrane
BP	Band-pass
BS	Band-stop
CI	Cochlear implant
CN	Cochlear nucleus
CNS	Central nervous system
DCN	Dorsal part of Cochlear Nucleus
DTF	Directional transfer function
DMF	Dynamic movement field
FEF	Frontal eye fields
FM	Frequency modulation
FOV	Field of view
FRF	Future receptive field
FT	Fourier transform
GBC	Globular bushy cell
GME	Gaze-motor error
GWN	Gaussian white noise
HA	Hearing aid
HP	High-pass
HRTF	Head-related transfer function
HSE	Head-shadow effect
IC	Inferior colliculus
ICc	Central nucleus of IC
ICx	External nucleus of IC
IHC	Inner hair cell
ILD	Interaural level difference
INC	Interstitial nucleus of Cajal
IOR	Inhibition of return
IPD	Interaural phase difference

ISI	Intersaccadic interval
ITD	Interaural time difference
LP	Low-pass
LS	Linear system
LSO	Lateral superior olive
LT	Laplace transform
MAA	Minimum audible angle
MAP	Maximum a-posteriori
MDT	Medial-dorsal thalamus
MF	Movement field
MGB	Medial geniculate body
MI	Multisensory Index
MLB	Medium-lead burst neuron
MLE	Maximum Likelihood Estimate
MNTB	Medial nucleus of the trapezoid body
MSO	Medial superior olive
MVN	Medial vestibular nucleus
NI	Neural integrator
NLS	Nonlinear system
NPH	Nucleus prepositus hypoglossi
OAE	Oto-acoustic emission
OHC	Outer hair cell
OMR	Oculomotor range
OPN	Omni-pause neuron
PG	Pulse generator
PPC	Posterior parietal cortex
PPRF	Para-pontine reticular formation
PSG	Pulse-step generator
PVCN	Postero-ventral part of Cochlear Nucleus
riMLF	rostral interstitial nucleus of the medial longitudinal fasciculus
RM	Reissner's membrane
ROC	Receiver operator characteristic
RT	Reaction time
SBC	Spherical bushy cell
SC	Superior colliculus
SDT	Signal-detection theory
SNR	Signal to noise ratio
SPL	Sound-pressure level
SR	Spontaneous firing rate
SRT	Saccade reaction time
SSD	Single-sided deaf(ness)
STT	Spatial-to-temporal transformation
TM	Tectorial membrane
TOT	Tonotopic to oculocentric transformation
UCHL	Unilateral Conductive Hearing Loss
VOR	Vestibular-ocular reflex
VPG	Vectorial pulse generator
VS	Vector strength

Chapter 1

A Brief Introduction to the Topic

1.1 TWO TASKS FOR THE AUDITORY SYSTEM

Whenever a detectable sound wave reaches our ears, the brain will try to assign meaning to the acoustic event. In a split second, the auditory system succeeds in *identifying* the nature of the sound source out of a virtually unlimited number of possibilities: is it noise (the wind, the rain, the sea, a sigh)? Was it perhaps a familiar or an unfamiliar human voice? Was it an animal vocalization? Maybe it was a car, some other man-made machine, a musical instrument, or an orchestra? Perhaps, the sound was caused by the ticking of an object (a fork?) against another object (a dinner plate?), etc.

At the same time, the auditory system *localizes* the sound source. But just like source identification, the seemingly simple localization task could refer to multiple possibilities: where is the sound source located in "external space," that is, in the world around us, through which we navigate? Or: where is the sound relative to the ears or head? Where is it relative to other landmarks in the environment? Surprisingly, as we will see later, the brain seems to be particularly interested in determining where the sound source is located *relative to your eyes*! Thus, the auditory system has evolved to perform the following major tasks on the acoustic input:

Auditory task	It answers
Identification	What?
Localization	Where?

Obviously, the ability to rapidly identify and localize sound sources is vital for survival. In any case, it was crucial when in a not too distant past, we as hominids, had to struggle fiercely to stay alive, as food sources (good for us) and predators (very bad for us) had to be identified and localized as fast as possible. It is therefore not surprising that throughout evolution, the auditory systems of virtually all the animal species have developed dedicated neural circuits to efficiently and accurately solve identification and localization tasks.

Although simply formulated, these tasks are in fact astonishingly difficult to perform. Current technological advances, despite the tremendous increase in computer speed and memory storage over the last decades, are still not able to execute these tasks with the same accuracy, speed, flexibility, and efficiency as biological

The Auditory System and Human Sound-Localization Behavior. http://dx.doi.org/10.1016/B978-0-12-801529-2.00001-5

Chapter 5

The Cochlea

5.1 INTRODUCTION: FROM ACOUSTIC INPUT TO TRAVELING WAVE

The acoustic pressure signal that drives the motion of the tympanic membrane and middle-ear bones (see chapter: The Nature of Sound), results in an amplified vibratory motion of the stapes, which is attached to the oval window at the cochlear *base*. The cochlea is filled with an ionic fluid that can flow between the interconnected bony structures of the cochlea and vestibular canals (Fig. 5.1). The cochlea is divided into three chambers, separated from each other by bony walls, and called *Scala Vestibuli, Scala Media*, and *Scala Tympani*, respectively (Fig. 5.4). The partitions are connected at the far end of the cochlea (the *apex*), by an opening, known as *helicotrema*.

The movements of the stapes exert a time varying–inward outward directed force at the basal end of the Scala Vestibuli (Fig. 5.2). Because fluid is incompressible, the resulting pressure is released with an opposite sign at the elastic *round window* at the base of the Scala Tympani. This means that across the *Scala Media*, the absolute *pressure difference* between Scala Vestibuli and Scala Tympani varies from a maximum value at the cochlear base (at oval and round windows), to zero at the helicotrema, which acts as a pressure short-circuit. It is this time-varying pressure difference across the length of the central cochlear partition, $\Delta p(x,t)$, which acts as the *driving force* for hearing. For a pure tone, that is, a harmonic sound with frequency ω rad/s, the pressure from the stapes on the fluid at the base of the Scala Vestibuli ($x = 0$) is described by

$$p_{\text{base}}(t) = A_{\text{base}} \sin(\omega t) \tag{5.1}$$

with A_{Base} the pressure amplitude at the base. The pressure *difference* at the cochlear base is then given as (Fig. 5.3):

$$\Delta p_{\text{base}}(t) = 2A_{\text{base}} \sin(\omega t) \tag{5.2}$$

Along the cochlear partition (with coordinate, x), this pressure difference gradually falls to zero when it reaches the apex (in the human cochlea, at about

The Auditory System and Human Sound-Localization Behavior. http://dx.doi.org/10.1016/B978-0-12-801529-2.00005-2

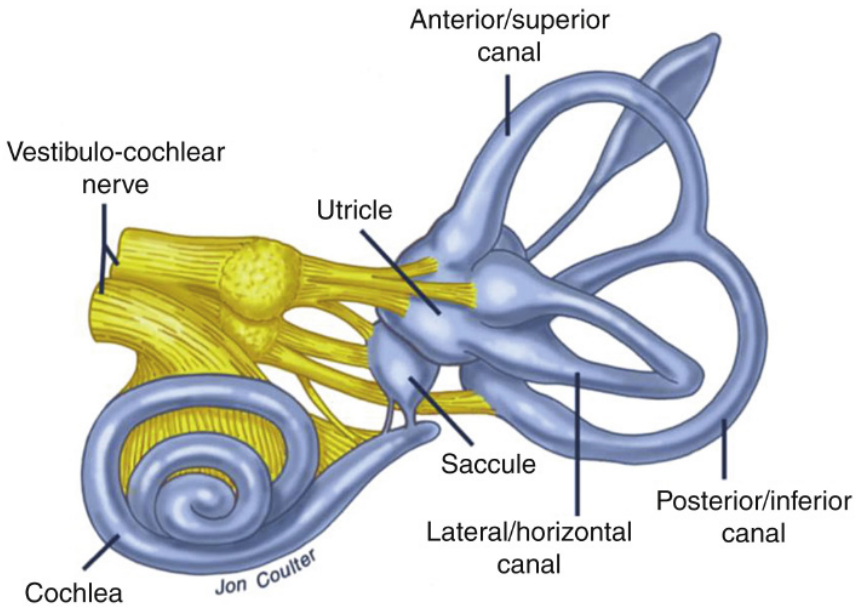

FIGURE 5.1 The bony structures of the inner ear. It shows the vestibular organs (the three semicircular canals, which measure three-dimensional head rotations, and the otoliths: saccule and utricle, which respond to linear head accelerations and gravity), and the cochlea, the sensory organ for audition. Output is transmitted to the CNS by auditory and vestibular nerves. *(Source: Jon Coulter, with kind permission.)*

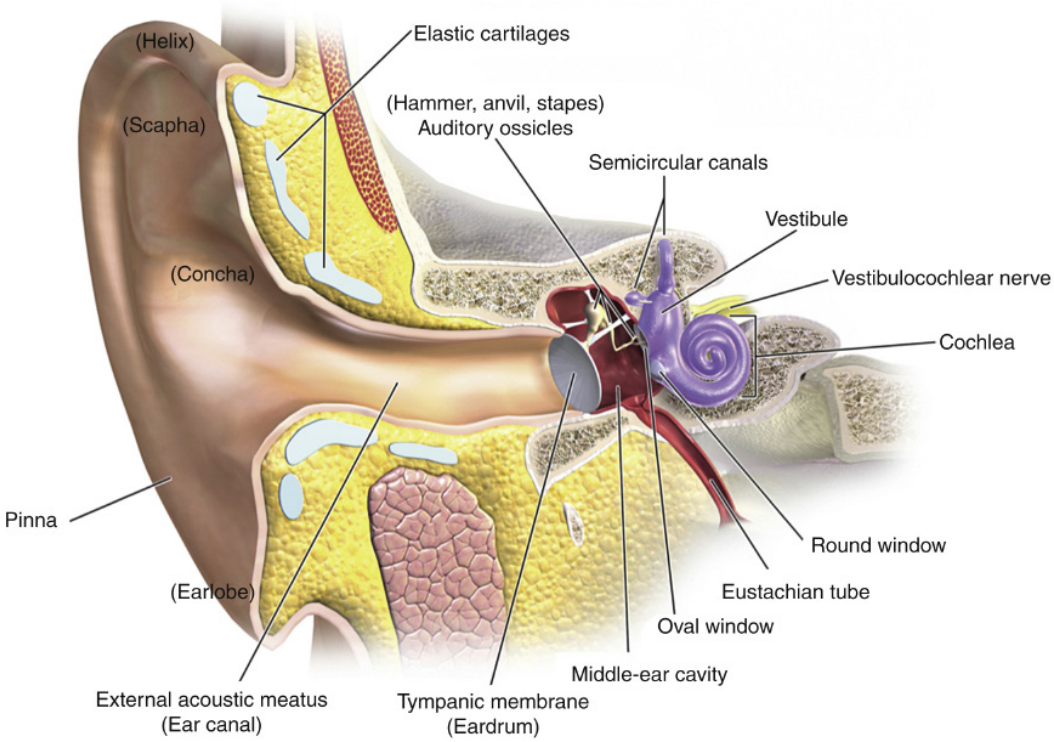

FIGURE 5.2 Anatomy of the ear: outer ear, middle ear, and cochlea. The cochlea is acoustically stimulated by the vibratory movements of the stapes at the oval window. The round window moves in antiphase with respect to the oval window. *(Source: Wikipedia.)*

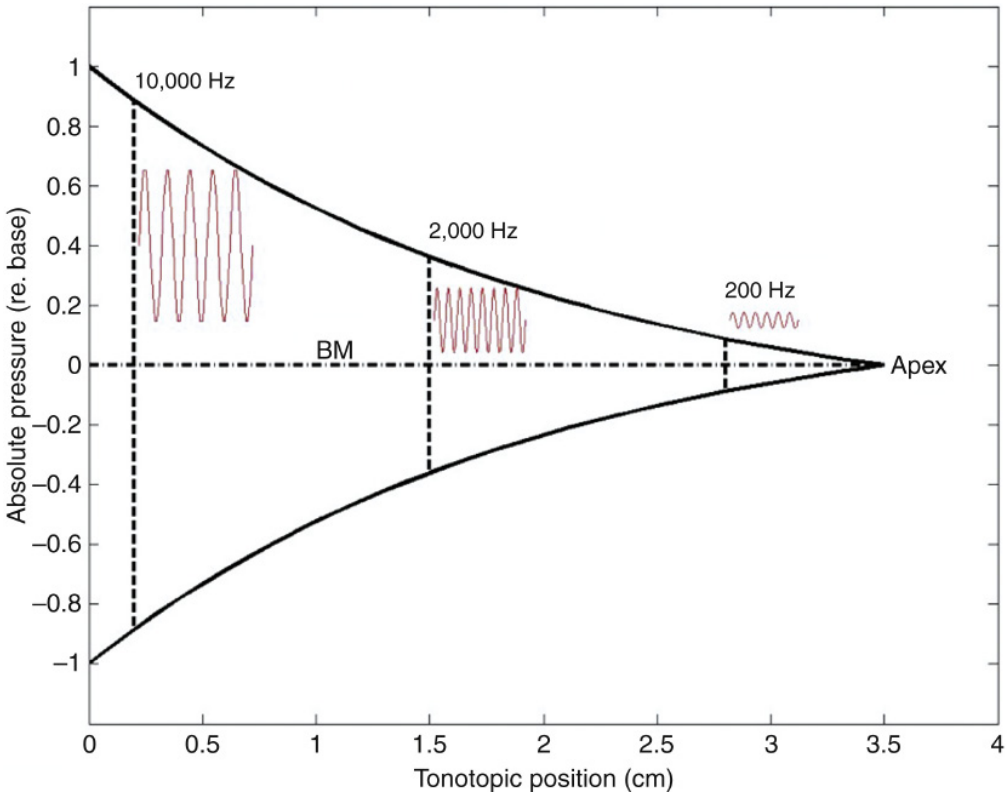

FIGURE 5.3 **The amplitude of the pressure across the BM decays with distance from the base at $x = 0$** [Eq. (5.4)]. The oscillating driving forces at different locations therefore have very different amplitudes too (here illustrated to scale for three frequencies at $x = 0.2$, 1.5, and 2.8 cm from the base; here: $\beta = 0.5$ cm^{-1}, and $x_{apex} = 3.5$ cm).

$x_{apex} = 3.5$ cm from the base), making the pressure difference strongly location-dependent. To give a first, very simple idea, it may appear like:

$$\Delta p(x,t) = 2A_{base}\, a(x) \sin(\omega t) \tag{5.3}$$

with $a(x)$ a function that decays monotonically from one to zero between base and apex (see Section 5.3, where we describe a full linear model for the cochlear hydro-dynamics). For example, if the pressure difference were to fall exponentially, with a spatial constant of β cm^{-1}, it would read (Fig. 5.3):

$$\Delta p(x,t) = 2A_{base} \frac{e^{-\beta x} - e^{-\beta x_{apex}}}{1 - e^{-\beta x_{apex}}} \sin(\omega t) \tag{5.4}$$

As the speed of sound in water is 1,500 m/s, the pressure along Scala Vestibuli and Tympani develops virtually instantaneously. However, due to the hydrodynamic interactions between the fluid and the acoustic impedance of the basilar membrane (BM), it takes about 5–6 ms for the time-varying pressure difference to develop along the cochlear partition from base to apex (Section 5.3).

The BM (Fig. 5.4) responds to the dynamic pressure difference with a vibratory motion that has the same frequency as the driving acoustic (pure-tone) input. Along the length of the cochlea, the envelope of the BM vibrations appears as a

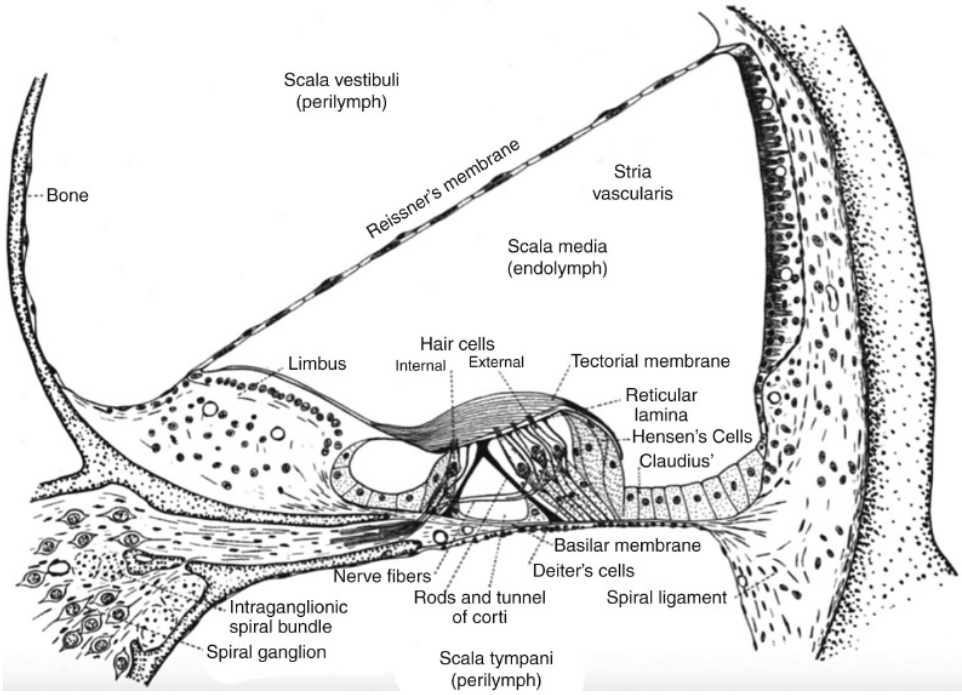

FIGURE 5.4 Cross section of the cochlear partition, showing the organ of Corti within Scala Media. Important structures are the BM, the inner hair cell, the three outer hair cells (OHCs) and the tectorial membrane to which the OHCs' stereocilia attach. Reissner's membrane is considered acoustically transparent; Scala Media and Scala Vestibuli form a single acoustic compartment. *(Source: Davis and Associates, 1953, with kind permission).*

traveling wave that propagates from base to apex (Fig. 5.5) with a group velocity that depends on the location along the BM, $v_g(x)$, and an envelope amplitude that gradually grows to its peak at a frequency-dependent location, $A_{peak}(x)$: high-frequency harmonics peak near the BM base, while low-frequency tones reach

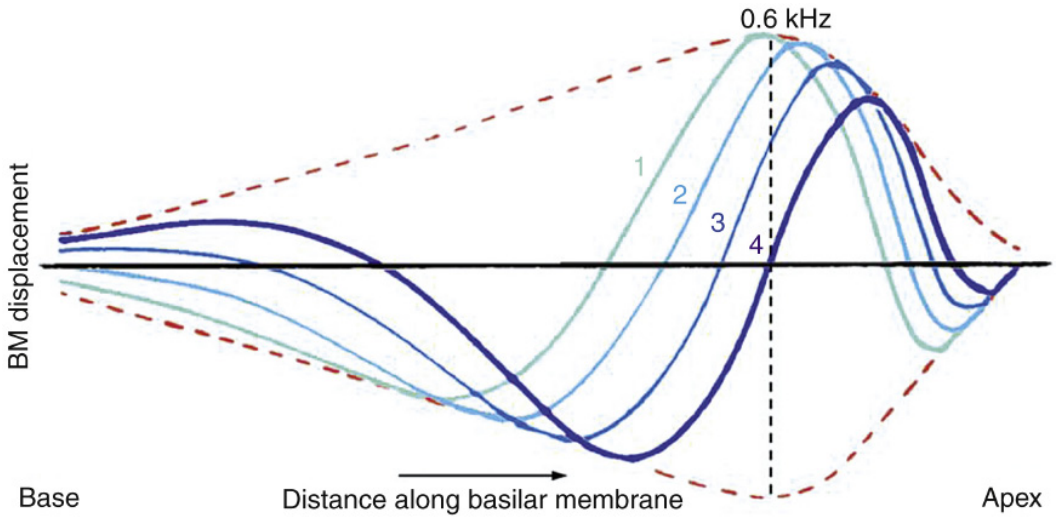

FIGURE 5.5 A pure-tone sound causes a traveling wave that propagates along the BM from base to apex. The wave reaches its peak amplitude at a frequency-dependent location, after which it quickly drops to zero. Here the wave is shown at four time points. The *red dashed line* delineates the wave's envelope. Note the change of the wavelength along the length of the BM, which cooccurs with a systematic decrease in the wave's group velocity, until it comes to a full stop beyond the peak.

their peak amplitude near BM apex. The wave amplitude quickly drops to zero beyond the peak.

The time it takes for the traveling wave to reach its peak amplitude varies with location too. Relative to the cochlear base, the lowest frequencies near the BM apex reach their peak amplitude about 5–6 ms later, which leads to substantial *dispersion* of the acoustic signal when it contains multiple frequencies!

These interesting properties of the traveling wave all result from location-dependent properties of the BM impedance. In first (ie, *linear*) approximation, the BM responds to the local pressure variations as a second-order, damped oscillator (chapter:Linear Systems; see also further, Section 5.5), with a location-dependent elasticity (or: compliance, C): $Z(\omega) = Z[\omega, C(x,\omega)]$.

As a result of these local micromechanics, sound frequencies are mapped *tonotopically* along the BM, from high (base) to low (apex), running (in the human inner ear) from $f_{max} \approx 20$ kHz, down to $f_{min} \approx 50$ Hz. The tonotopic mapping is not linear, but may be approximated by a logarithmic function, in which each doubling (or halving) of the frequency (ie, at an octave interval) occupies a roughly constant spatial extent on the BM of about $\lambda \approx$ 4–5 mm. An approximate description for the tonotopy may therefore be (Fig. 5.6):

$$x_{BM} = -\lambda \log_2 \left(\frac{f}{f_{max}} \right) \text{ cm} \tag{5.5}$$

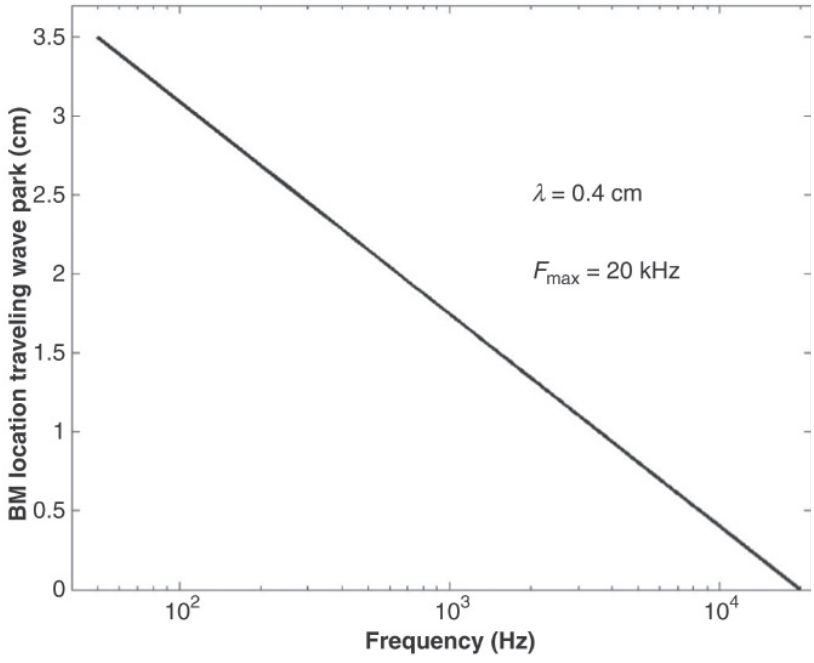

FIGURE 5.6 The tonotopy along the BM may be approximated by Eq. (5.5). Here, $\lambda = 0.4$ cm, and $f_{max} = 20$ kHz.

The BM wave dynamics are quite different from the simple (nondispersive) constant-amplitude and constant velocity traveling waves that arise, for example, in an elastic spring or a rope under constant tension, or in air with a constant bulk modulus (as outlined in chapter: The Nature of Sound), as such mechanical systems obey the simple homogeneous and nondispersive wave equation, Eq. (2.25).

Perhaps a better way to describe the BM traveling wave would be that of a shallow-water wave that breaks on the beach: in such water waves, the wave velocity strongly depends on depth, so that these waves obey a nonlinear dispersion relation. As the wave velocity decreases with decreasing depth (impedance), the wave amplitude increases (because of the incompressibility of water), until the wave crest topples over and breaks. The properties of water waves result from a few basic physical principles that apply to fluids (ie, in easily deformable, but incompressible media). The next section summarizes some of the interesting physics underlying traveling shallow-water waves, as a nice metaphor for the BM traveling wave.

5.2 BASIC PHYSICS UNDERLYING WATER WAVES

The tsunamis that devastated South-East Asia on Christmas eve 2004 (Fig. 5.7), and more recently on Mar. 11, 2011 near Sendai, in Japan, gave new meaning to the concept of "water waves." In the beginning, the story went that waves of many meters high had traveled over the ocean at a tremendous speed. However, the actual tsunami wave in the middle of the ocean is usually not high at all (typically, only several tens of cm, and hardly noticeable if you happen to be on a boat), but the wave crest extends over a vast distance (easily extending over a few hundred kilometers!). Moreover, the speed of this traveling, pulse-shaped, wave is about

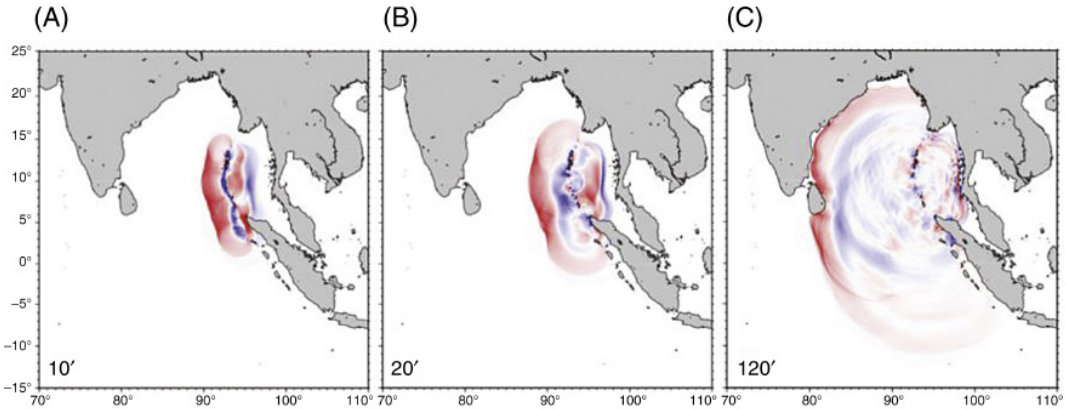

FIGURE 5.7 The tsunami in the Indian Ocean caused by an extremely strong earthquake on the ocean floor at a depth of about 5 km near Sumatra on Christmas eve, 2004. The three consecutive shots (taken from NASA satellite observations) show the amplitude of the traveling wave (*red*, positive; *blue*, negative) at respectively (A) 10 min, (B) 20 min, and (C) 120 min after the onset of the earthquake. The speed of this nondispersive "shallow"-water wave is about 1000 km/h, and its wavelength is several hundred kilometers long. Note the reflective waves (*blue*) that bounce off the small islands as given in part B. *(Source: dr Kenji Satake, Tokyo, with kind permission).*

800–1000 km/h (ie, over 250 m/s!). When such a tsunami approaches the coast, the wave crest becomes higher and higher, while its speed decreases strongly. Finally, the wave breaks on the coast, thereby transferring an enormous amount of mechanical energy. What are the physical mechanisms behind this type of waves?

Here we spend a brief time on the physics underlying water waves. Although the model will be strongly simplified, it will nevertheless be quite useful to understand the most important properties of water waves. Some of these properties are also relevant for understanding the basic hydrodynamics within the cochlea that are described in the next section, and to appreciate the nondispersive traveling wave described earlier.

Dry water. The first simplification in the physical model of water waves is that of so-called "dry," nonviscous, water, which means that we ignore internal friction between the different water layers. We will further limit the description to relatively small wave amplitudes, evoked by a harmonic, sinusoidal, perturbation. Third, we assume that the water wave propagates essentially in one dimension (the x-direction): this allows for a description of a straight wave front, parameterized by a single wavelength, in which the peaks and valleys follow straight, parallel lines, perpendicular to the propagation direction in the (x,z)-plane. We will see that despite these simplifications the dispersion relation of the water waves, $\omega(k)$, with $k = 2\pi/\lambda$ the wave number, can be nonlinear (Crawford, 1968).

At equilibrium the water surface is flat and horizontal. When a perturbation causes a wave, two restoring forces will cause the peaks of the wave to return to equilibrium: gravity, g, and the surface tension, T, of the water. Moreover, because water is incompressible, the excess of water in the wave's peak has to come from neighboring troughs. As a result, the water particles (here described as tiny water volumes, think of infinitesimal "droplets") will undergo combined *longitudinal* and *transversal* movements. We will derive the following properties of water waves:

- when the water depth $h \ll \lambda$ we speak of *shallow-water waves*, or tidal waves. The particles will move along straight lines, and the wave speed is independent of λ, only depending on h (nondispersive waves).
- when $h \gg \lambda$ we have *deep-water waves*. Now, the particles move in circles with a radius that depends on their equilibrium position in depth. Furthermore, the wave speed depends on λ (dispersive waves).

Consider an infinitely large reservoir at a uniform depth, h. In equilibrium the water surface is horizontal, and lies in the plane $y = 0$; the bottom is at $y = -h$. Position (x,y) refers to the *equilibrium* position of a water particle, where $x \in [-\infty,+\infty]$ and $y \in [-h,0]$. A water drop is thus conveniently labeled by its equilibrium location, irrespective of where it actually is during the wave motion. The water wave is a 2D movement of particles within in the (x,y)-plane (we may ignore the z-direction), which is described by a wave-vector function:

$$\vec{\psi}(x,y,t) = \psi_x(x,y,t)\,\hat{x} + \psi_y(x,y,t)\,\hat{y} \tag{5.6}$$

with $\hat{x}$ the longitudinal movement direction of the particle, and $\hat{y}$ its transversal movement direction. The speed of the water droplet at (x,y) is therefore:

$$\vec{u}(x,y,t) = \frac{\partial \vec{\psi}(x,y,t)}{\partial t} = \frac{\partial \psi_x}{\partial t}\hat{x} + \frac{\partial \psi_y}{\partial t}\hat{y} \equiv v\hat{x} + w\hat{y} \tag{5.7}$$

We now impose two important physical boundary conditions on the dry water:

1. Conservation of mass, and
2. Absence of turbulent motion (rotation-free water).

The first condition uses the incompressibility of water, and states that the total amount of water that enters and leaves a certain water-filled volume per unit of time should be zero. This constraint leads to the *continuity equation*, which for motion in 2D (the x–y plane) reads:

$$\rho\left[\frac{\partial v}{\partial x} + \frac{\partial w}{\partial y}\right] = \rho\left(\vec{\nabla}\vec{u}\right) = 0 \tag{5.8}$$

with ρ the density of water, and $\vec{u} = (v,w)$ is the velocity of the water particles in the x and y directions, respectively. Using Eq. (5.7) yields

$$0 = \rho\left(\vec{\nabla}\frac{\partial \vec{\psi}}{\partial t}\right) \Rightarrow \left(\vec{\nabla}\vec{\psi}\right) = \text{constant} = 0. \tag{5.9}$$

The integration constant is zero, because the water volume is assumed to be homogeneous (ie, there are no "air bubbles").

The second condition means that at infinitesimal scale there is no net rotation in the flow field of the liquid, which is mathematically formulated as:

$$\vec{\nabla}\times\vec{u} = 0 \Rightarrow \vec{\nabla}\times\vec{\psi} = 0 \quad \text{and in} \quad \text{2D:} \left(\frac{\partial \psi y}{\partial x} - \frac{\partial \psi x}{\partial y}\right)\hat{z} = 0 \tag{5.10}$$

The two constraints of Eqs. (5.9) and (5.10) provide the necessary boundary conditions to determine solutions for harmonic traveling waves. We therefore propose as tryout solutions for the horizontal and vertical components of the wave vector:

$$\begin{aligned} \psi_y(x,y,t) &= \mathrm{A}\cos(\omega t - kx) f(y) \\ \psi_x(x,y,t) &= \mathrm{A}\sin(\omega t - kx) g(y) \end{aligned} \tag{5.11}$$

where the unknown functions $f(y)$ and $g(y)$ should be determined by imposing the constraints of Eqs. (5.9) and (5.10). It is left as an Exercise to the reader to show that the full solution then is given by:

$$\begin{aligned} \psi_y(x,y,t) &= \mathrm{A}\cos(\omega t - kx)\left[e^{ky} - e^{-2kh}e^{-ky}\right] \\ \psi_x(x,y,t) &= \mathrm{A}\sin(\omega t - kx)\left[e^{ky} + e^{-2kh}e^{-ky}\right] \end{aligned} \tag{5.12}$$

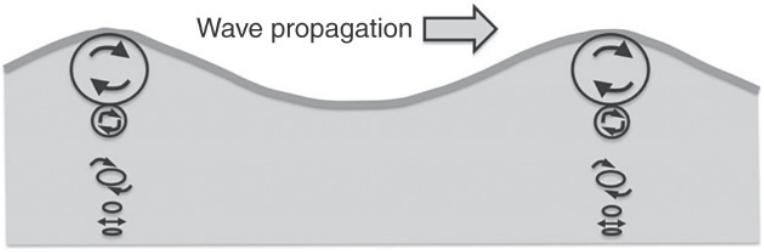

FIGURE 5.8 Movement of individual water particles in a deep-water harmonic traveling wave at different depths.

This wave function predicts *elliptic trajectories* for the water particles, where the longitudinal movement along the wave-propagation direction (x) is harmonic, and the transversal movement (y) depends on the location of the particle, on the wavelength, and on the basin depth (Fig. 5.8). To get more insight into the behavior of the water particles, we highlight two extreme cases: very short versus very long wavelengths with respect to the depth, h. The former case refers to *deep-water* waves, the latter to *shallow-water* waves. The general solution of Eq. (5.12) incorporates these two extremes.

Deep-water waves: When $h \ll k$, the factor containing $\exp(-2kh) \ll 1$ and may be neglected. In that case

$$\begin{aligned} \psi_y(x,y,t) &= \mathrm{A}\cos(\omega t - kx)e^{ky} \\ \psi_x(x,y,t) &= \mathrm{A}\sin(\omega t - kx)e^{ky} \end{aligned} \tag{5.13}$$

which describes harmonic *circular* motion of the water particles, with a radius that decreases exponentially with y (note that $y < 0$!). At the top op the wave crest the particles move forward, while in a trough they move backward. Note that $\exp(ky) = \exp(-|y| / \bar{\lambda})$ where $\bar{\lambda} \equiv \lambda / 2\pi$ is the *reduced* wavelength (Fig. 5.8).

Shallow-water waves: In this case $y \ll \bar{\lambda}$ and $h \ll \bar{\lambda}$, which leads to the following solution (see Exercises):

$$\begin{aligned} \psi_y(x,y,t) &= 2\mathrm{A}\cos(\omega t - kx)\cdot k(y+h) \\ \psi_x(x,y,t) &= 2\mathrm{A}\sin(\omega t - kx) \end{aligned} \tag{5.14}$$

This reduces to purely horizontal particle motion on the bottom of the reservoir (where $y = -h$), and to elliptical motion on the surface (where $y = 0$).

Dispersion relation: To get at the dispersion relation for water waves we have to incorporate the forces that act on the water particles. Two forces play a role in dry water waves: gravity, g, and surface tension, T (where we neglect viscosity as a third force). We use the fact that for general harmonic motion (be it a pendulum, an electric circuit, water, etc.) the following statement holds (Crawford, 1968):

> The total restoring force per unit displacement per unit mass = ω^2.

For example, Newton's second law describes the (linearized) pendulum (Eq. 3.4) by:

$$ML\frac{d^2\psi}{dt^2} = -Mg\psi$$

from which the harmonic solution yields $\omega^2 = g/L$. This can also be written as:

$$\omega^2 = \frac{Mg\psi}{(L\psi)M} = \frac{\text{restoring force}}{\text{unit of displacement} \times \text{mass}}$$

For a given vibrational mode of the water waves, all particles have the same frequency, and hence the same ω^2. Thus, we can obtain the dispersion relation between the spatial wave mode (k) and the driving frequency (ω), by analyzing the movements of a single water particle.

Gravitational waves: In case the gravitational forces dominate the surface tension, we have so called *gravitational* water waves.

The highlighted gray volume of water in Fig. 5.9 undergoes a force that is proportional to the pressure difference along x: $\Delta p(x) = p(x + \Delta x) - p(x)$. This pressure gradient is caused by the difference in height (and hence by the volume) of the water, determined by the wave shape: $\psi_y(x + \Delta x) - \psi_y(x)$.

In other words:

$$\begin{aligned} F_x &= -L\Delta y p(x) \\ &= -L\Delta y \rho g\left[\psi_y(x+\Delta x) - \psi_y(x)\right] \\ &\approx -\Delta M g \frac{\partial \psi_y}{\partial x}\Big]_{y=0} \end{aligned} \tag{5.15}$$

The partial derivative is obtained from the general spatial solution of the traveling water waves, Eq. (5.12). The restoring force equals the

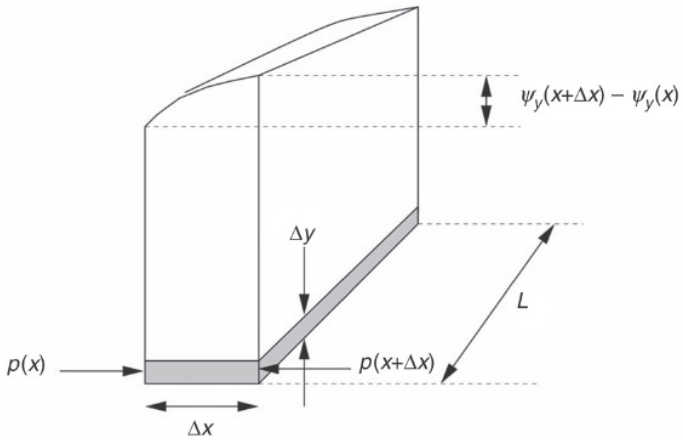

FIGURE 5.9 A small volume of water (Δx,Δy,L) at depth y, subjected to the pressure from the force of gravity by the water volume above it. The pressure difference is due to the mass of the wave crest, and is given by $\rho g \Delta \psi_y$.

acceleration on the mass, ΔM, and for harmonic motion at frequency ω, this yields

$$F_x = \Delta M \left. \frac{\partial^2 \psi_x}{\partial t^2} \right]_{y=0} = -\Delta M \omega^2 \psi_x \Big]_{y=0} \tag{5.16}$$

Combining the results gives the dispersion relation for gravitational waves:

$$\omega^2(k) = gk \frac{1 - e^{-2kh}}{1 + e^{-2kh}} = gk \tanh(kh) \tag{5.17}$$

In the Exercises the reader can show that the phase velocity, $v_\varphi = \omega/k$, is then given by:

- for deep-water waves:

$$v_\varphi = \sqrt{g\bar{\lambda}} \text{ (dispersive waves)} \tag{5.18}$$

- for shallow-water waves:

$$v_\varphi = \sqrt{gh} \text{ (nondispersive waves)} \tag{5.19}$$

Deep-water waves are dispersive: when the wave is determined by a superposition of multiple frequencies, its shape will change as the wave progresses. For shallow-water waves the shape is preserved, as the different frequencies all travel at the same phase velocity that only depends on (assumed constant) depth. The tsunami should therefore be considered a *shallow-water wave*, despite the fact that the depth at which it originates may be 5 km or more! This explains why tsunamis can propagate unchanged over vast distances across the ocean (Fig. 5.7), and why they are so rare….

Surface tension: At the transition between water and air, where the water molecules lose their tight bonds to each other, and bond to air molecules, the water surface behaves somewhat as a stretched elastic membrane. This membrane resists deformation, and hence the restoring force is proportional (by tension constant, T) to the amount of deformation from a flat surface, which is quantified by the surface *curvature*. For a sinusoidal wave shape, the curvature is k^2 (to be checked in the Exercises), so that the restoring force due to the surface tension of a sinusoidal shape becomes:

$$F_x = -\Delta M \left. \frac{Tk^2}{\rho} \frac{\partial \psi_y}{\partial x} \right]_{y=0} \tag{5.20}$$

Combining both the influence of gravity and surface tension eventually leads to a more complete dispersion relation for water waves (see Exercises):

$$\omega^2(k) = \left(gk + \frac{Tk^3}{\rho} \right) \tanh(kh) \tag{5.21}$$

Depending on the strength of the tension, T, the shallow-water wave can become dispersive, as with the approximation $hk \ll 1$ and $\tanh(kh) \approx kh$:

$$\omega^2(k) \approx \left(ghk^2 + \frac{Thk^4}{\rho} \right) \Rightarrow \omega(k) = k\sqrt{gh + \frac{Th}{\rho}k^2} \tag{5.22}$$

The phase- and group velocities thus become:

$$\begin{aligned} v_\varphi &\equiv \frac{\omega(k)}{k} = \sqrt{gh + \frac{Th}{\rho}k^2} = v_\varphi(k) \\ v_g &\equiv \frac{d\omega}{dk} = v_\varphi + \frac{2Th\dfrac{k^2}{\rho}}{v_\varphi} = v_g(k) \end{aligned} \tag{5.23}$$

In the typical situation, however, the terms containing Thk^2 can be neglected, so that the phase velocity is independent of the wavelength, only depending on the depth, h, and phase- and group velocities are identical. This describes non-dispersive waves, as long as h = constant. However, if h varies, the propagation velocity of the wave will change too.

5.3 THE LINEAR COCHLEAR MODEL (VON BÉKESY AND ZWISLOCKI)

To develop a hydrodynamic model of the cochlea, we follow the approach of Josef Zwislocki, who incorporated the Nobel Prize-winning experimental work of Georg Von Békésy (1961, Nobel Prize in *Physiology or Medicine*; Fig. 5.10).

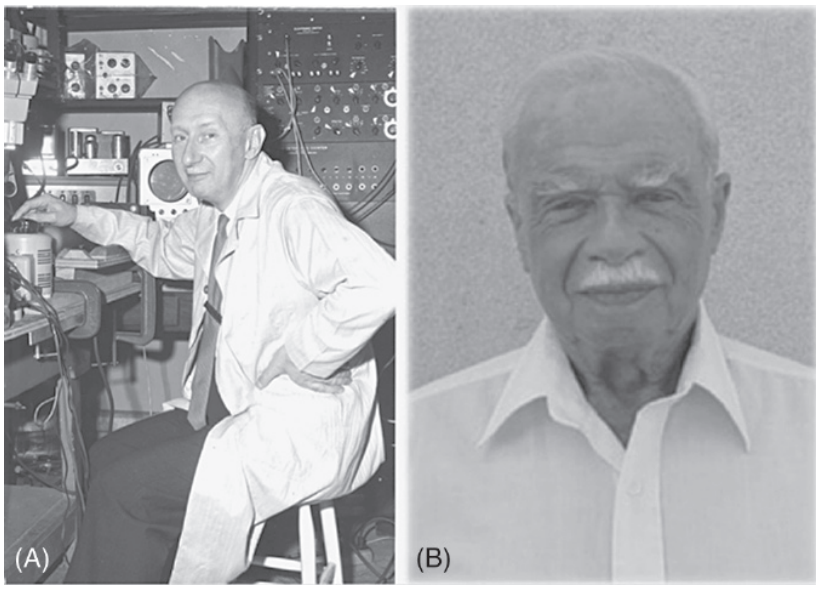

FIGURE 5.10 **Géorg Von Békésy 1899–1972, (A) and Josef J. Zwislocki (B).**

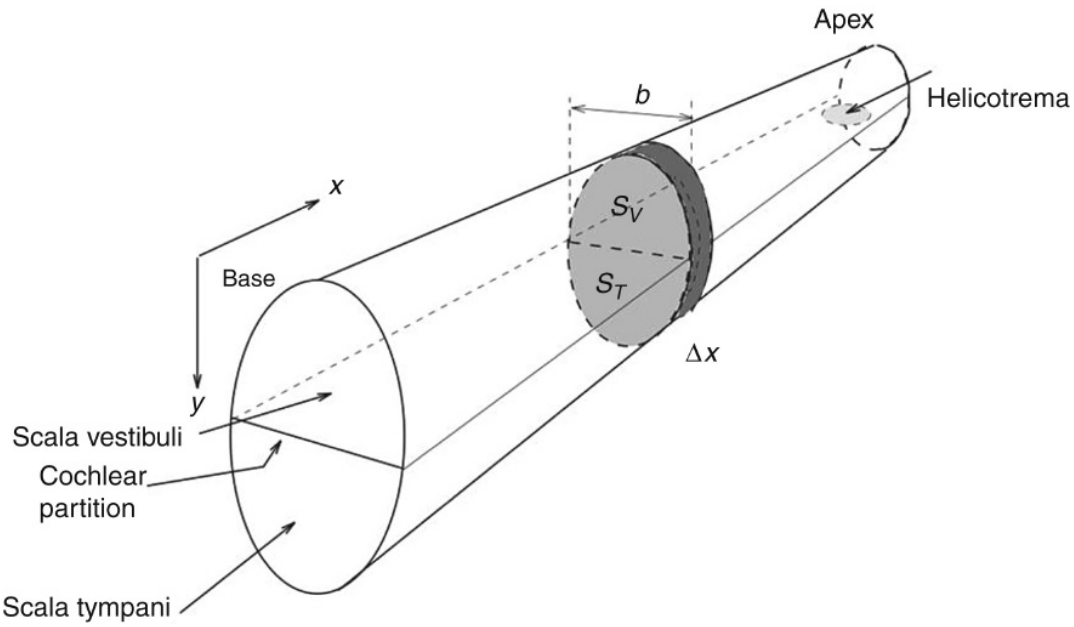

FIGURE 5.11 Schematic representation of the physical model of the cochlea. S_V, Scala vestibuli; S_T, scala tympani. The scalas are separated by the cochlear partition (BM, width b). At the apex the scalas are connected by the helicotrema. The highlighted part at location x, has length Δx, width $b(x)$, and scala cross sections $S_V(x)$ and $S_T(x)$.

In this model we imagine the cochlea as a linearly stretched compartment (Fig. 5.11). The input signal is the in- and outward movement of the stapes plate at the oval window. The cochlea is filled with fluid, and separated (for cross section, see Fig. 5.3) by a triangular structure, called the cochlear partition, or *organ of Corti*. In cochlear models this partition is flattened to represent an elastic, centrally running partition (the BM with supporting structures) between Scala Vestibuli (S_V) and Scala Tympani (S_T). In other words, Reissner's membrane (RM) does not interact with the acoustic hydrodynamics within the cochlea (it is acoustically transparent); as a result, the fluid within Scala Media can be incorporated within the compartment of Scala Vestibuli [see, however, recent evidence from Reichenbach et al. (2012), implicating RM in oto-acoustic emissions]. At the apex, the two compartments are connected by the helicotrema. When the stapes moves inward, the round window at the base of S_T moves outward. All elastic properties of the central partition are assigned to the BM: a high stiffness near the stapes (the base), decreasing gradually toward the helicotrema (apex).

The movements of the BM can be measured with the Mössbauer technique, or with laser interferometry. Measured speeds at the threshold of hearing are of the order of 0.05 mm/s at a frequency of 20 kHz; this corresponds to BM displacements of only 4 Å (check!).

We consider one-dimensional fluid motion, in which the compression wave propagates from the oval window in the x-direction toward the helicotrema. Locally, the fluid particles have velocity $v(x)$. In what follows, we apply continuity Eq. (5.9), which describes mass conservation.

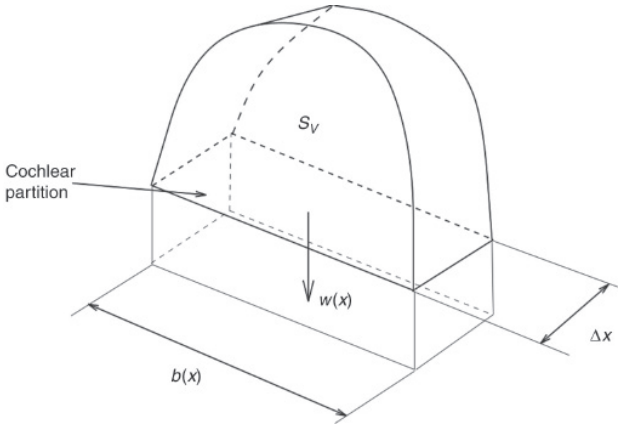

FIGURE 5.12 Scheme of the local volume change at x in the scala vestibuli due the up–down movement $w(x)$ of the BM. As an approximation, we consider the BM movement as a linear displacement, that is, without a change in shape of the partition.

Fig. 5.12 shows a schematic cross section of the Scala Vestibuli at location x along the BM. All variables are location-dependent: the width of the BM, $b = b(x)$, the cross section $S_V = S_V(x)$, and $S_T = S_T(x)$, the (horizontal) velocity of the fluid, $v(x)$, and the BM is supposed to move linearly upward and downward at velocity, $w(x)$. Note that what happens to the BM in S_T is a mirror image of what happens in S_V.

The mass-inflow per time unit to the volume element in S_V at location x is equal to the change in volume (velocity times cross section) times the density (which is constant because of incompressibility):

$$\Delta m(x) = v_V(x) S_V(x)(x) \rho \tag{5.24}$$

and at location $x + \Delta x$, to which we apply a first-order Taylor expansion:

$$\begin{aligned} \Delta m(x+\Delta x) &= v_V(x+\Delta x) S_V(x+\Delta x) \rho \\ &= \left[v_V(x) + \frac{\partial v_V}{\partial x} \Delta x \right] \left[S_V(x) + \frac{\partial S_V}{\partial x} \Delta x \right] \rho \\ &= \Delta m(x) + \rho \frac{\partial}{\partial x} (v_V S_V) \Delta x \end{aligned} \tag{5.25}$$

The net change in mass resulting from the pressure wave is therefore:

$$\Delta M^x(x) = m(x) - m(x+\Delta x) = -\rho \frac{\partial}{\partial x} (v_V S_V) \Delta x \tag{5.26}$$

The volume change as a result of the BM movement equals $w(x)b(x)\Delta x$, so that the change in mass per unit time for the vertical movement (in Fig. 5.11 the membrane moves downward, so a mass increase for S_V):

$$\Delta M^y(x) = \rho w(x) b(x) \Delta x \tag{5.27}$$

According to the continuity equation, the total mass change is zero:

$$\rho\Delta x\left[w(x)b(x)+\frac{\partial}{\partial x}(v_V S_V)\right]=0 \tag{5.28}$$

For Scala Tympani, we obtain a similar condition, with only the BM velocity inverted:

$$\rho\Delta x\left[-w(x)b(x)+\frac{\partial}{\partial x}(v_T S_T)\right]=0 \tag{5.29}$$

To determine the relation between BM movement, $w(x)$, and the pressure wave in the cochlea, we have to analyze the force balance on the volume elements in S_V and S_T. The three forces that play a role in this problem are the *net pressure* on the volume element, the *inertia* (Newton's second law), and the *viscous forces* on the fluid. Since the volume element does not accelerate through the cochlea, the sum of these forces adds to zero. First, we consider S_V:

1. Suppose that the pressure in x is $p_V(x)$, then the force at the cross-sections in x and $x + \Delta x$ is, in first-order Taylor approximation:

$$\begin{aligned} F_V^p(x) &= p_V(x)S_V(x) \\ F_V^p(x+\Delta x) &= p_V(x)S_V(x)+\frac{\partial(p_V S_V)}{\partial x}\Delta x \\ \Rightarrow F_V^{\Delta p}(x) &= -\frac{\partial(p_V S_V)}{\partial x}\Delta x \approx -S_V\frac{\partial p_V}{\partial x}\Delta x \end{aligned} \tag{5.30}$$

   where the approximation holds when the cross-section varies slowly with x.
2. The impulse of the liquid in the volume element (mass × velocity) is $I(x)=\left[\rho S_V(x)\Delta x\right]v_V(x)$, so that according to Newton's law:

$$F_V^N(x)\equiv\frac{\partial I(x)}{\partial t}=\rho\frac{\partial(S_V v_V)}{\partial t}\Delta x\approx\rho S_V\frac{\partial(v_V)}{\partial t}\Delta x \tag{5.31}$$

   where the cross section is assumed to vary little over time.
3. In a viscous liquid the frictional force is proportional to the speed of the liquid particles:

$$F_V^{\text{visc}}(x)=-\left[R_V(x)S_V(x)\right]v_V(x)\Delta x \tag{5.32}$$

   with $R_V S_V$ is the total resistance per unit length.

The force balance thus reads:

$$F_V^N(x)-F_V^{\Delta p}(x)-F_V^{\text{visc}}(x)=0 \tag{5.33}$$

and reduces to:

$$\rho\frac{\partial v_V}{\partial t}+R_V v_V=-\frac{\partial p_V}{\partial x}\quad\text{together with}$$
$$wb+S_V\frac{\partial v_V}{\partial x}=0 \tag{5.34}$$

The force balance and continuity equation for S_T gives a very similar result, as the only difference is the sign of the movement, w, of the BM:

$$\rho\frac{\partial v_T}{\partial t}+R_T v_T=-\frac{\partial p_T}{\partial x}$$
$$-wb+S_T\frac{\partial v_T}{\partial x}=0 \tag{5.35}$$

These coupled differential equations can be readily uncoupled by applying the following trick: differentiate the force equation with respect to x, and the continuity equation with respect to t. We further assume that the resistance varies slowly with x, so that its spatial derivative may be neglected. Adding the two equations then gives for each of the two compartments (but check):

$$-\frac{b}{S_V}\left(\rho\frac{\partial w}{\partial t}+R_V w\right)=-\frac{\partial^2 p_V}{\partial x^2}$$
$$+\frac{b}{S_T}\left(\rho\frac{\partial w}{\partial t}+R_T w\right)=-\frac{\partial^2 p_T}{\partial x^2} \tag{5.36}$$

If we now take the difference between S_V and S_T, approximate that $R_V = R_T \approx R$, and define the effective cross section $(1/S) = (1/S_V) + (1/S_T)$, we get:

$$\frac{b}{S}\left(\rho\frac{\partial w}{\partial t}+Rw\right)=-\frac{\partial^2 \Delta p}{\partial x^2} \tag{5.37}$$

where $\Delta p(x,t)$ is the instantaneous pressure difference across the BM, and $w(x,t)$ is the BM velocity. These two quantities are related through Eq. 2.46:

$$p(x,t)=b(x)w(x,t)Z(x,\omega) \tag{5.38}$$

This relation allows us to eliminate the BM velocity, leading to an equation that only contains the instantaneous pressure difference:

$$\frac{1}{SZ(x,\omega)}\left[\rho\frac{\partial \Delta p(x,t)}{\partial t}+R\Delta p(x,t)\right]=\frac{\partial^2 \Delta p}{\partial x^2} \tag{5.39}$$

This is the central equation of cochlear hydrodynamics, with a minimum of approximations and assumptions. Note that Eq. (5.39) a *linear* differential equation in the pressure difference, so that it describes essentially a *linear* cochlear model! Despite this apparent oversimplification, the equation is still quite complex, as S, Z, and R are all functions of x. This makes an analytical treatment of Eq. (5.39) far from trivial.

Zwislocki's approximations: To analyze Eq. (5.39), Zwislocki made a number of simplifying assumptions and substitutions, taken from the experimental findings of Von Békésy.

As discussed in chapter: Linear Systems, linear systems can often best be dealt with in the frequency (or Laplace) domain. In that case, we assume that the sound input is a harmonic signal. In complex notation this is conveniently written as:

$$\Delta p(x,t) = P(x)e^{i\omega t} \tag{5.40}$$

Substitution into Eq. (5.39), and collecting the terms then yields

$$\frac{(R+i\rho\omega)}{SZ(x,\omega)} = \frac{1}{P}\frac{d^2P}{dx^2} \tag{5.41}$$

and using the impedance relation, Eq. (5.38), gives an equation for the BM velocity:

$$\frac{b(R+i\rho\omega)}{S} = \frac{1}{W}\frac{d^2W}{dx^2} \tag{5.42}$$

To arrive at the total displacement of the BM as function of distance to the stapes, $y(x)$, we integrate $w(x,t)$ after taking the inverse FT:

$$y(x) = \int_0^t w(x,\tau)d\tau \text{ and in the frequency domain: } Y(\omega) = \frac{W(x,\omega)}{i\omega} \tag{5.43}$$

Zwislocki proposed a number of physical-realistic descriptions for $R(x)$, $S(x)$, and $Z(x,\omega)$. For example, Fig. 5.13A suggests that the cochlear cross-section as function of the distance to the oval window can be reasonably well approximated by an exponential function:

$$S(x) = S_0 e^{-ax} \quad \text{with} \quad S_0 \approx 0.0125 \text{ cm}^2 \quad \text{and} \quad a \approx 0.5 \text{ cm}^{-1} \tag{5.44}$$

Analysis of the experimental results of the viscous component led to:

$$R(x) = R_0\sqrt{\omega}e^{-ax^2} \quad \text{with} \quad R_0 \approx 2.24 \text{ (g/cm)}^3\text{s}^{-0.5} \tag{5.45}$$

The most general model for the BM impedance proposes that a local membrane element has an equivalent *mass* $M(x)$, an *elasticity* (or

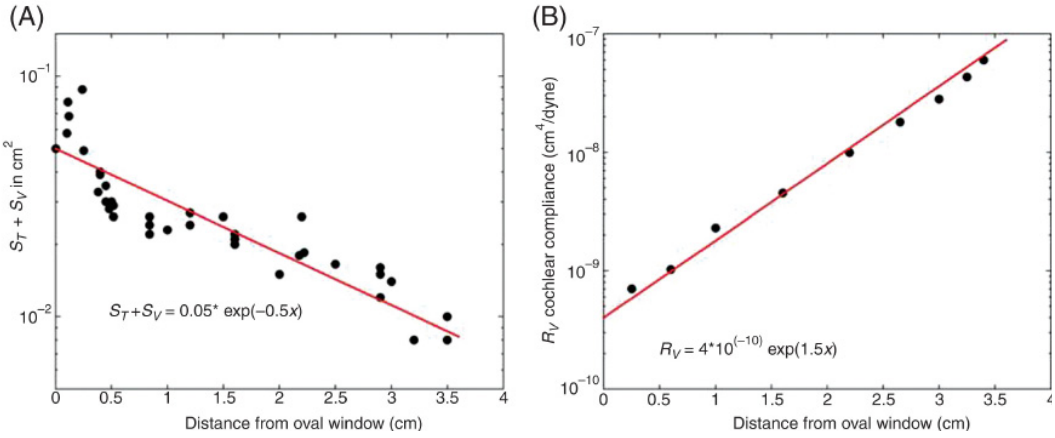

FIGURE 5.13 (A) Cross-section of scala vestibuli and scala tympani as a function of x for the human cochlea. (B) Static compliance of the BM as function of x.

compliance), $C(x)$, and a *damping* $R_m(x)$. The membrane impedance is then described by:

$$Z(x,\omega) = R_m(x) + i\left[\omega M(x) - \frac{1}{\omega C(x)}\right] \tag{5.46}$$

Following the measurements of Von Békésy, Zwislocki proposed the following approximations:

$$\begin{gathered} M(x) \approx 0 \\ R_m(x) \approx R_m = 468 \\ C(x) = C_0 e^{-hx} \quad \text{with } C_0 \approx 4\times10^{-10} \text{ cm}^4/\text{dyne}, \; h \approx 1.5 \text{ cm}^{-1} \end{gathered} \tag{5.47}$$

[for data on $C(x)$, see Fig. 5.13B]. Substitution of these experimentally inspired relations in Eq. (5.39) then yields the following, formidable equation:

$$\frac{1}{P}\frac{d^2P}{dx^2} = \frac{R_0\sqrt{\omega}\exp\left(\frac{ax}{2}\right) + i\omega\rho}{S_0\exp(-ax)\left[R_m - i\exp(-hx)/(\omega C_0)\right]} \tag{5.48}$$

Finally, after applying the following approximations (which were supported by numerical substitution of the measured values):

- $\omega R_m C_0 \ll 1$
- $R_0 R_m C_0 \ll \rho$
- $\omega R_m C_0 + R/(\omega\rho) \ll 1$

Eq. (5.48) then finally reduces to a relatively standard differential equation (Exercise):

$$-\frac{1}{P}\frac{d^2P}{dx^2} = \frac{\omega^2 C_0\rho}{S_0}e^{(h+a)x} \tag{5.49}$$

This equation can be transformed into a standard Bessel equation, for which analytical solutions are available.

The solution following from Eq. (5.49) (normalized to the pressure at the stapes, $x = 0$), after substituting the measured values, is eventually given by (Dallos, 1973):

$$\text{Amplitude: } |P(x,f)| = P_0 \exp\left[-\frac{1}{2}x - 6.7\times10^{-10} f^2\left(e^{2.5x}-1\right) - 1.84\times10^{-3}\sqrt{f}\left(e^{1.25x}-1\right)\right]$$
$$\text{Phase: } \Phi(x) = \Phi_0 - 1.12\times10^{-3} f\left(e^{x}-1\right) \qquad (5.50)$$

where x is in centimeters, and f in Hertz. The pressure amplitude decreases monotonically when both f and x increase. At a constant driving frequency, the amplitude of the pressure wave decreases in the direction of the helicotrema [where it becomes vanishingly small; cf. the highly simplified Eq. (5.3)].

At a fixed position, the pressure decreases with increasing frequency (Fig. 5.14). In other words:

- High frequencies give rise to a significant pressure amplitude over only a restricted range of the BM.
- Low frequencies cover a wider spatial range (Fig. 5.14A).
- Locations away from the stapes are progressively delayed. This phase-lag is strongly frequency-dependent (Fig. 5.14B).

The main quantity of interest, however, is the vertical displacement of the BM $y(f, x)$ (see previous sections), which can be obtained from the pressure wave by the impedance equation, Eq. (5.38), and subsequent integration, Eq. (5.43). Using the same approximations as above, the amplitude of the impedance yields:

$$\frac{1}{|Z|} \approx \omega C\sqrt{1+\omega^2 R_m C^2} \approx \omega C = 2\pi f \times 4\times10^{-10} e^{x} \qquad (5.51)$$

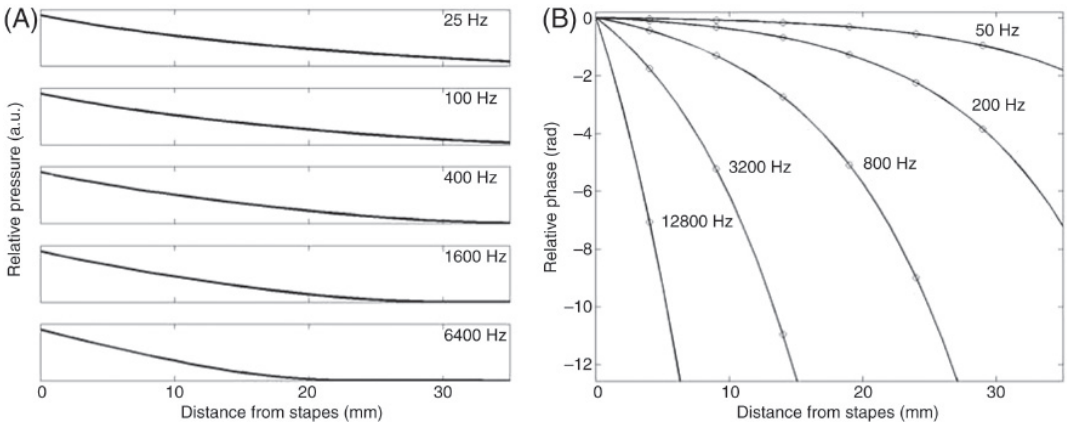

FIGURE 5.14 **Properties of the pressure wave.** Calculated according to Eq. (5.50) for five different frequencies: relative amplitude (A) and relative phase (B). Note the strong frequency- and location-dependence of both quantities.

The displacement of the BM is then [from Eq. (5.43)]:

$$|y(x,f)| = \frac{\omega C |P(x,f)|}{\omega}$$

This determines the relative amplitude of the BM traveling wave with respect to the stapes.

$$|y(x,f)| = |y(0,f)| \exp\left[x - 6.7\times10^{-10} f^2 \left(e^{2.5x} - 1\right) - 1.84\times10^{-3}\sqrt{f}\left(e^{1.25x} - 1\right)\right] \quad (5.52)$$

The phase of the BM displacement (with the used approximations) is equal to that of the pressure wave, Eq. (5.50). Fig. 5.15 shows that the linear model of Eq. (5.52) predicts a nice monotonic relationship between the location of the maximum of the traveling wave, and the driving frequency of the stapes. It demonstrates the asymmetry of the wave shape, with its steep roll-off, which has a similar appearance as a shallow water wave breaking on the beach (Section 5.2). It also accounts for the logarithmic tonotopy of the BM (right).

The cochlea thus functions as a mechanical frequency analyzer that acts as a tonotopically organized, parallel set of frequency specific–band pass filters. The temporal behavior of the BM vibration along the partition is best described as a *traveling wave*.

Note, however, that the wavelength is not constant along the partition, but decreases as a function of x. This behavior requires an analysis of the wave's

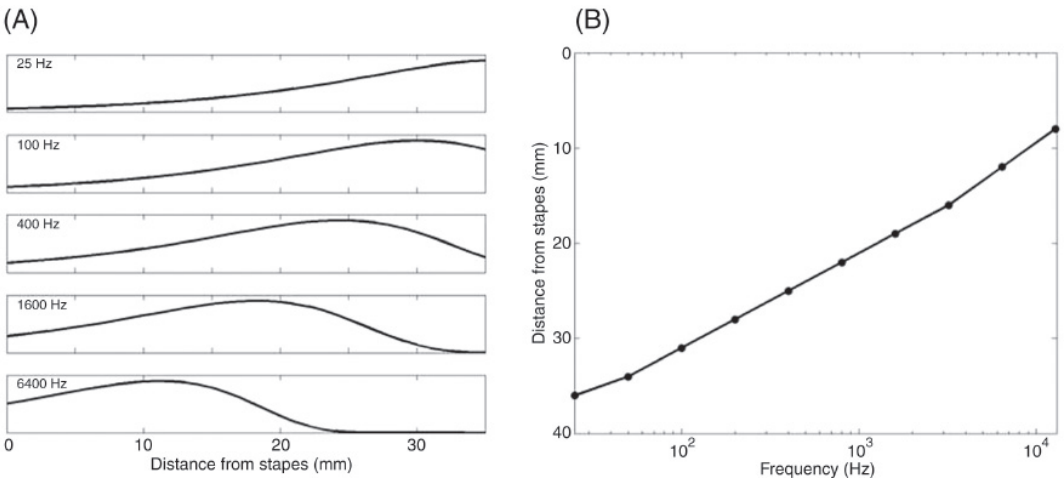

FIGURE 5.15 Envelope of the traveling wave along the length of the BM for five different frequencies, according to Eq. (5.52). Notice that the width of the wave, as well as the location of the peak systematically shifts with sound frequency (A). (B) Tonotopy along the BM for the peaks of the traveling wave (cf. with Fig. 5.6).

phase velocity (chapter: The Nature of Sound). The BM oscillates with $y(x,t)$, so that the phase velocity is defined by:

$$v_\varphi = \frac{dx}{dt} \tag{5.53}$$

The instantaneous phase of the traveling wave is determined by [making use of Eq. (5.50)]

$$\Phi(t) = \omega t + \Phi(x,\omega) = \omega t + \Phi_0 - 1.8\times10^{-4}\,\omega\left(e^x - 1\right) \tag{5.54}$$

from which the phase velocity is found by differentiation:

$$v_\varphi \equiv \frac{\partial\Phi(t)}{\partial t} = \omega - 1.8\times10^{-4}\,\omega e^x \frac{dx}{dt} \tag{5.55}$$

For locations that are precisely one wavelength apart, the phase is constant, so that $\partial\Phi/\partial t = 0$ yields the following important relation for the traveling wave:

$$v_\varphi = 5.6\times10^3 e^{-x} \quad \text{cm/s} \tag{5.56}$$

This interesting result demonstrates that:

- The propagation speed of the traveling wave toward the helicotrema decreases exponentially with distance from the base.
- The speed of the wave is independent of sound frequency.
- The time it takes for the wave to reach a given point, x_0, on the cochlea is $T_0 = 1.8\times10^{-4}(e^{x_0} - 1)$ s, taking about 5.7 ms to reach the helicotrema. This is in good agreement with the experimental observations of Von Békésy.

Note that according to the linear model, the traveling wave along the BM is entirely due to the interaction of *independent* BM elements with the local pressure difference in the fluid. The wave does not arise because BM elements transfer elastic energy in the longitudinal direction from one location to the next (like in a spring, in coupled oscillators, or in a rope); instead, the exchange of mechanical energy is with the local fluid only. Clearly, this description is an approximation of the real cochlear mechanics, as the membrane elements are connected to each other, and therefore must transfer mechanical energy. Yet, the simple linear model already yields realistic cochlear behavior, which is quite remarkable, and far from trivial. Moreover, it has important consequences for hearing. For example, if a certain portion of the BM cannot be set into motion, it will *not* affect the traveling wave!

Also a local rupture of the membrane, or ossification, leaves the traveling wave untouched. As a result, hearing of frequencies beyond the damage is unaffected! This has also been confirmed experimentally (eg, the "disco dip" at around 4 kHz).

5.4 THE ACTIVE, NONLINEAR COCHLEA: ROLE OF OUTER HAIR CELLS

Despite the apparent success of the linear cochlear model it cannot deal with some real fundamental problems. For example, Fig. 5.15 indicates that the extent of the traveling wave around the maximum of the BM vibration occupies about 1/3 of the total cochlear partition, which suggests that

1. fibers in the auditory nerve should be very broadly tuned, and
2. frequency selectivity of the auditory system is quite poor.

However, the frequency resolution of the human auditory system is actually very high (better than 0.5% over the full frequency range from 50 to 20 000 Hz). To measure the frequency selectivity of a given BM location one can determine its *tuning curves*, which quantify how the local amplitude of the vibration depends on the (relative) frequency.

Fig. 5.16 shows the normalized mechanical tuning curves, measured at five different BM locations by Von Békésy (apical data), and with the Mössbauer technique by Johnstone and Boyle (1967; at 18 kHz). The tuning curves clearly appear as band-pass filters, whereby their widths decrease with increasing frequency.

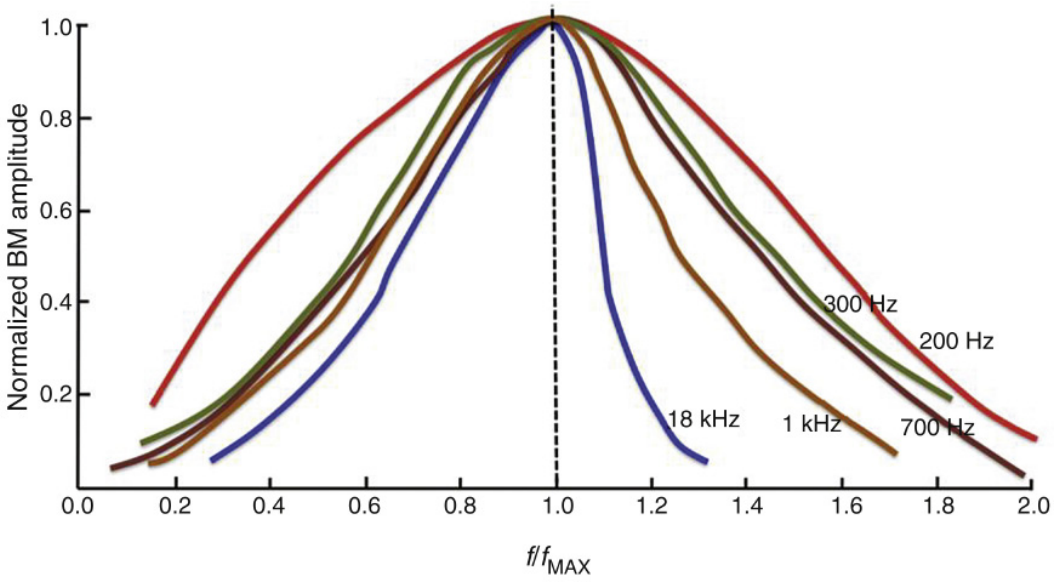

FIGURE 5.16 **Normalized mechanical tuning curves for different cochlear positions as reported by Johnstone and Boyle (1967).**

The effective bandwidth of a filter is quantified by its Q-factor, which is defined by:

$$Q_{10\,\mathrm{dB}} \equiv \frac{f_{\max}}{BW_{10\,\mathrm{dB}}} \tag{5.57}$$

with $\mathrm{BW}_{10\ \mathrm{dB}}$ the bandwidth at 10 dB below the maximum response. The linear model predicts Q-factors between 1.0 and 2.5; the measured BM data in Fig. 5.16 suggest Q-factors up to 3.5.

However, when comparing the (passive) BM filters to the tuning curves of auditory nerve fibers ($Q_{10\ \mathrm{dB}} \sim 8.5$), a dramatic difference is evident (Fig. 5.17A). In particular, the low-frequency slope of the BM filter is far too low, and nerve fiber tuning curves are much sharper than predicted from the BM tuning characteristics.

A second feature that cannot be explained by the linear model concerns the extreme sensitivity of the auditory system, especially for stimuli at very low intensities. Moreover, responses saturate when the stimulus levels become too high.

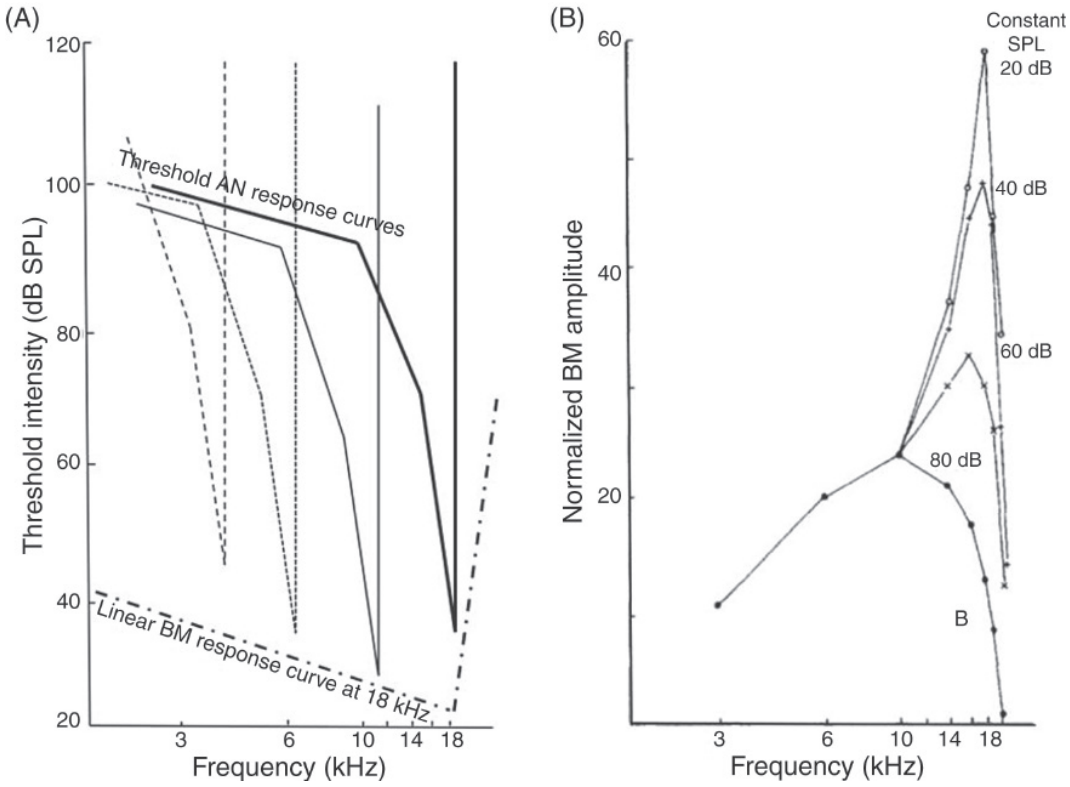

FIGURE 5.17 (A) Stylized tuning curves of four primary auditory nerve fibers, compared to the BM tuning curves (dotted line at the bottom). (B) Normalized gain functions of the BM for a 18.5 kHz tone presented at four different sound levels, between 20 and 80 dB SPL. The gain is defined as the BM velocity divided by the stapes input velocity. Note strong sharpening of the tuning curves at the lowest sound levels, indicative of nonlinear behavior. Note also the systematic shift of the peak to a higher best frequency, that is, to a more basal BM location, suggesting that the nonlinearity boosts the BM vibration at about 1/3–1/2 octave closer to the cochlear base than the passive tuning curve. *(Source: After Johnstone et al., 1986, with kind permission).*

These properties suggest the presence of a profound nonlinearity, as linear models do not produce different sensitivities for different sound levels, as the output scales linearly with the input strength (chapter: Linear Systems). Moreover, the nonlinearity appears to betray an *active* mechanism, as the highly increased sensitivity (high gain, in combination with sharpening of the BM tuning curve) may not be achievable by passive, dissipative, mechanisms without adding extra energy.

Indeed, measurements of the BM movements in the living cochlea with the Mössbauer technique demonstrated the existence of a spectacularly increased sensitivity for low sound levels, and saturation (stimulus-independent sensitivity, hence a linear response) for high levels (Fig. 5.17B). In the dead cochlea, however, these different response regimes disappear: in that case the BM again behaves as a linear system.

These important observations call for an essential modification of the linear Von Békésy–Zwislocki model. A crucial element in the nonlinear response behavior of the living cochlea is the involvement of outer hair cells (OHCs). Fig. 5.18B shows a magnified cross section of the organ of Corti with the inner (IHC) and OHCs.

The human cochlea contains about 12,000 OHCs and 3,500 IHCs. Against each IHC there are three OHCs. The flat top of the hair cells is covered with hair

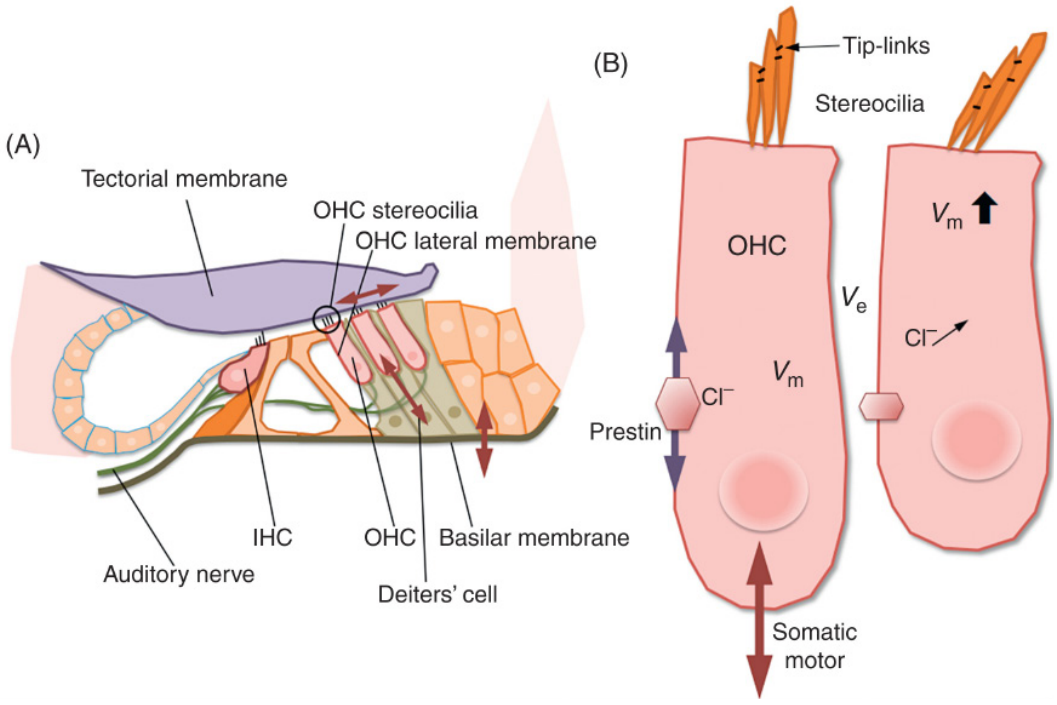

FIGURE 5.18 (A) Detailed cross section of the cochlear partition arrows indicate longitudinal and transversal movement directions of tectorial membrane, OHCs, and BM, respectively. (B) Different transduction mechanisms could underlie the OHC's somatic motor response: movement of the stereocilia, in combination with a rapid configuration change of prestin molecules. The resulting potential change across the cell length induces a motor response (length change) of the cell which in turn provides mechanical feedback (force) to the scala vestibuli/tympani.

bundles (*cilia*), which are made of sturdy filaments. On the OHC the cilia are arranged according to a wedge-shaped V or W form. Due to the fluid motion, the hair cell bundles can pivot around their pedestal. The resulting mechanical change of angle of the stereocilia causes a change of the internal potential of the hair cell. In the IHC this potential change can lead to the production of action potentials in the primary auditory nerve, according to the Hodgkin–Huxley spike-generation mechanism.

However, in the OHC the bending of the cilia induces a *length change* of the cell (Fig. 5.18B). This so-called *electro-motility* of the OHC has the *same* frequency as the acoustic signal that caused the cilia to bend, and it has in *in vitro* recordings that been established the motility responses can exceed well over 20 kHz (Scherer and Gummer, 2004)! As a result, the fast motion of the OHC can have an immediate effect on the vibratory motion of the BM, which was primarily induced by the traveling wave. In other words, the OHCs could provide a selective, local mechano-acoustic feedback to the BM, which is strongly frequency-selective (and could thus embody the long-sought active filter).

A further remarkable observation is that the *rest length* of the OHC is uniquely related to the resonance frequency of its mechanical response. Long OHCs are found near the apex, they have long cilia, and are mechanically tuned to low frequencies. At the base, the OHCs are short, are tuned to high-frequencies, and have short cilia (Brendin et al., 1989; Fig. 5.19A). Interestingly, these relationships, which do not apply to the IHCs, extend across many different species (Dannhof et al., 1991; Fig. 5.19C). Whether this relationship has a functional role in the OHC feedback mechanism, however, is not known.

It is thought that OHC mechanical feedback to the BM could act as a *positive* feedback, by locally amplifying the BM motion (ie, by providing *negative damping*). This mechanism causes increased sensitivity for low-intensity sounds, given that the OHC motility also depends on the absolute sound level through an additional efferent *neural* feedback pathway from the superior olive in the brainstem. It is therefore generally assumed, albeit still heavily debated (Ashmore et al., 2010), that the motor-mechanism of the OHCs forms the basis for the extreme sensitivity and selectivity of the cochlea. Fig. 5.20 provides a physical representation of the cochlear amplifier, as proposed by Nobili et al. (1998).

To model the role of the OHCs in the living cochlea, Nobili et al. (1998) proposed the following formalism. The idea is that the organ of Corti (BM and supporting structures) forms an uncoupled chain of position-dependent oscillators that interact with the surrounded fluid, and undergo a nonlinear local feedback from the electro-motility response of OHCs.

We saw in chapter: Linear Systems that the basic equation of motion for a second-order damped oscillator (here taken at location x_n, and not coupled through a medium) is:

$$m_n \frac{d^2 y_n}{dt^2} + \gamma_n \frac{dy_n}{dt} + k_n y_n = f_n(t) = -G_n a_s(t). \tag{5.58}$$

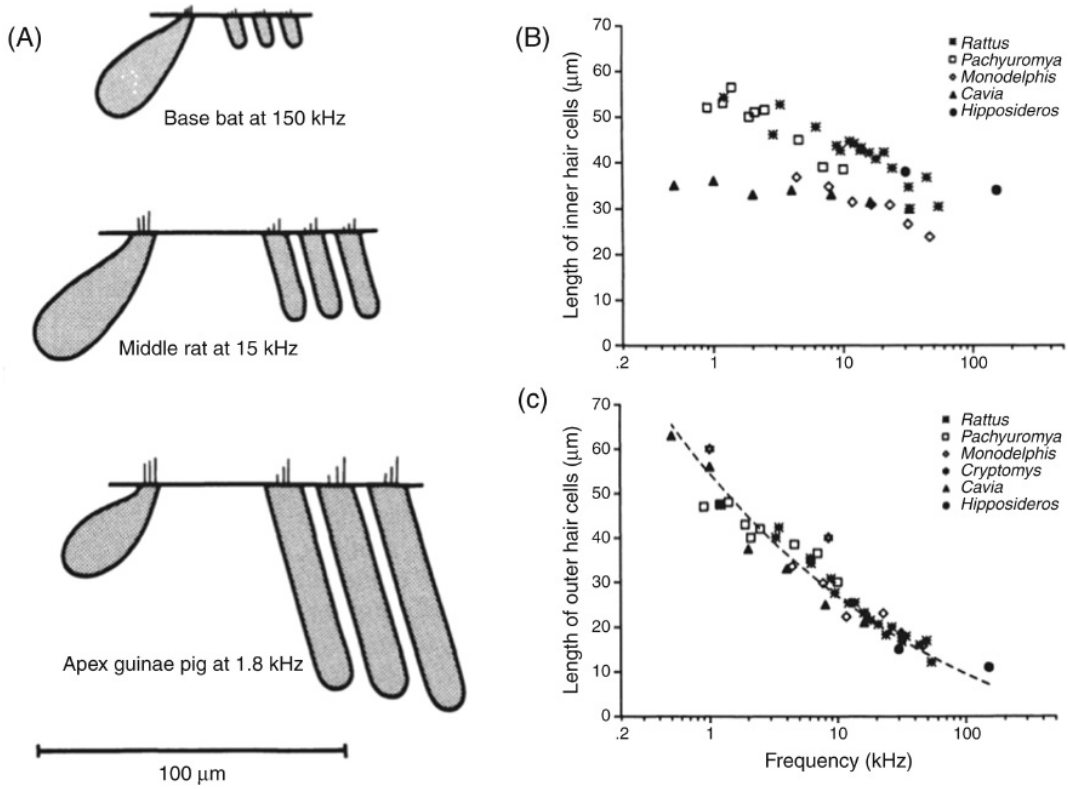

FIGURE 5.19 (A) The length of OHCs relates to their best frequency. Three examples from three different species (bat, rat, and guinea pig), taken from different locations along the BM. (B) The best frequencies of IHCs do not relate in a unique way to their size. (C) For OHCs, however, the same quantitative relation is found across species. *(Source: After Dannhof et al., 1991, with kind permission.)*

with m_n, γ_n, and k_n the local mass, viscosity, and elasticity of the oscillator at (discretized) location n. The external driving force, $f_n(t)$, is proportional to the (negative) acceleration of the stapes, $a_s(t)$, which is transmitted through the fluid as a local force to the oscillator (it is amplified by a local constant G_n, which is reminiscent to the pressure drop shown in Fig. 5.3).

In a more realistic cochlear model, however, the fluid at nearby locations does provide additional (*passive*) forces to the oscillator at n: (1) the resulting lateral hydrodynamic forces lead to motion of N oscillators at nearby sites, j, which in turn influence the oscillator at site n through (negative) fluid coupling (Fig. 5.21) and (2) shear forces that are due to differences in velocity of the fluid particles around the BM site. Together, these hydrodamic couplings provide the mechanism for Von Békésy's traveling wave (developed in Section 5.3), as illustrated in Fig. 5.21B.

In addition, the OHCs provide a feedback force, OHC_n, which opposes the dissipative damping through the electro-motility of the OHC cell body. This motility follows the rapid synchronized motion of the cell's stereocilia that undergo a displacement $z_n(t)$. The positive feedback (ie, effective negative damping) to the BM is mediated via the supporting Deiters' cells (Fig. 5.20A). Taken

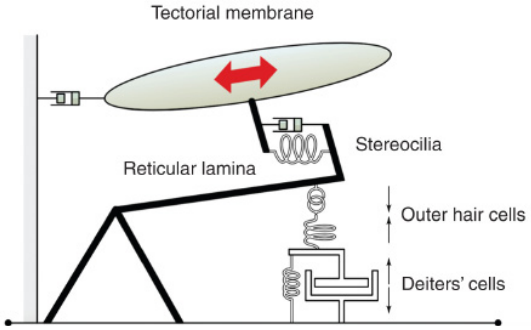

FIGURE 5.20 Physical model of the Organ of Corti (cf. with Figs. 5.4 and 5.18A), describing the coupling of OHCs to the BM. *(Source: Nobili et al., 1998, with kind permission.)*

together, the equation of motion of the *active* cochlear partition at site n thus reads:

$$\sum_{j=1}^{N}(G_n^j + m_n\delta_n^j)\frac{d^2y_j}{dt^2} + \gamma_n\frac{dy_n}{dt} + \mathrm{OHC}_n(z_n) + k_n y_n + s_n\left(2\frac{dy_n}{dt} - \frac{dy_{n+1}}{dt} - \frac{dy_{n-1}}{dt}\right) = -G_n a_s(t) \tag{5.59}$$

where δ_n^j is the Kronecker delta (it is 1 for $j = n$, and 0 otherwise) (Fig. 5.21).

Fig. 5.17B shows how the location of the excitatory peak of an auditory nerve fiber systematically shifts in the basal direction (to higher frequencies) for lower sound levels. The total shift over an 80 dB intensity range amounts to 1/3–1/2 octave, and suggests that the feedback mechanism of the cochlear

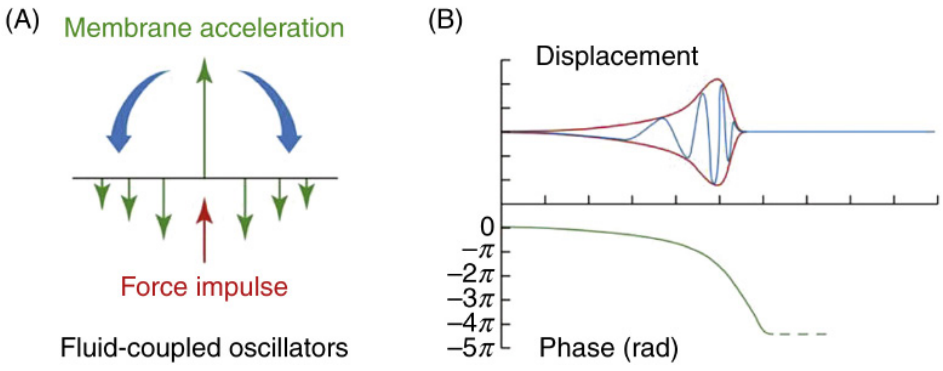

FIGURE 5.21 (A) A force impulse applied locally at BM site n (*red arrow*) leads to an instantaneous acceleration of the BM element, but also to an oppositely directed hydrodynamically mediated force (*blue arrows*) to nearby sites (*downward green arrows*). (B) Because of location-dependent mechanical properties of the BM (modeled as an exponential decay of its stiffness), the resulting BM movement is a traveling wave. The wavelength of the oscillations decreases from base to apex, reaching a critical point at a location that depends on the driving frequency (right). The phase delay (*green curve*) increases with distance from the stapes. *(Source: Nobili et al., 1998, with kind permission.)*

amplifier is in fact generated by a *second* set of tuned filters. Clearly, these filters involve a role for the OHCs, but it has been suggested that the coupling occurs between OHCs in combination with the mechanical properties of the tectorial membrane (TM). The TM attaches firmly to the long stereocilia of OHCs, and is in turn influenced by BM motion through hydrodynamic coupling (Fig. 5.22). Further, also the elastic TM can behave as an oscillator (eg, Zwislocki and Kletsky, 1979; Russell et al., 2007; see also Fig. 5.18A). Following Eq. (5.59), this behavior can thus be described as:

$$m_n^{\mathrm{TM}} \frac{d^2 z_n}{dt^2} + \gamma_n^{\mathrm{TM}} \frac{dz_n}{dt} + k_n^{\mathrm{TM}} z_n = -C_n \frac{d^2 y_n}{dt^2} \tag{5.60}$$

with C_n a constant local hydrodynamic coupling. Note that at resonance $(m_n^{\mathrm{TM}})[(d^2 z_n)/(dt^2)] = -k_n^{\mathrm{TM}} z_n$ (Newton's second law), so that Eq. (5.60) reduces to:

$$z_n = -\frac{C_n}{\gamma_n^{\mathrm{TM}}} \frac{dy_n}{dt} \tag{5.61}$$

As a result, at resonance (ie, locally, and driven by the pure tone acoustic input) the displacement of the stereocilia can indeed lead to a *negative damping* (ie, amplification) of the BM motion (Fig. 5.23).

Two mechanisms could underlie the remarkable high-frequency mechanical response of the OHC, which could presumably work together: (1) the cell-body motility induced by prestine proteins, which provides the feedback force to the BM, and (2) the stereocilia themselves that could drive the cell contractions at the correct phase (Ashmore et al., 2010; Fettiplace and Hackney, 2006; Hudspeth, 1985; Hudspeth 2014).

Yet, despite the in vitro evidence of high-frequency OHC responses, it still remains to be established whether the cochlear amplifier results from an active mechanism [that adds energy (negative damping) to the BM; Dallos, 1992;

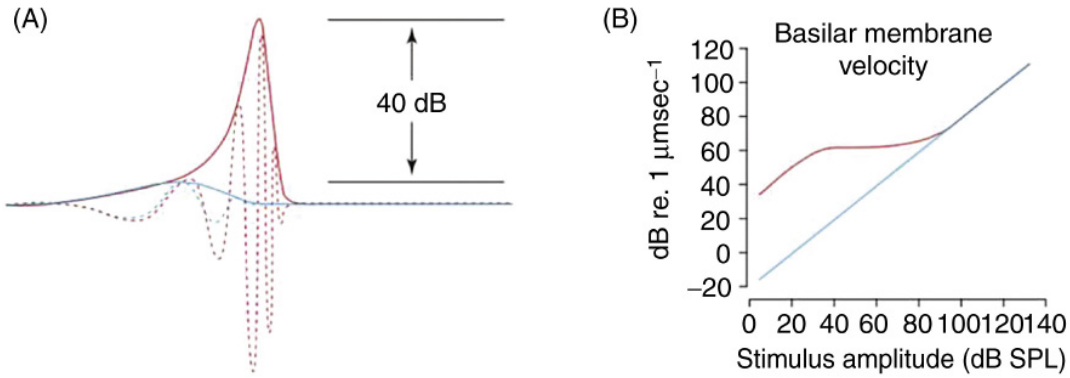

FIGURE 5.22 (A) Effect of the cochlear amplifier (OHC gain) on BM motion for a low-intensity sound, at high OHC gain (*red curve*), and at low gain (*blue curve*). (B) The *blue curve* shows the linear BM response (independent of sound level); the *red curve* shows the result of a level-dependent (saturating) gain of OHC feedback. *(Source: Nobili et al., 1998, with kind permission.)*

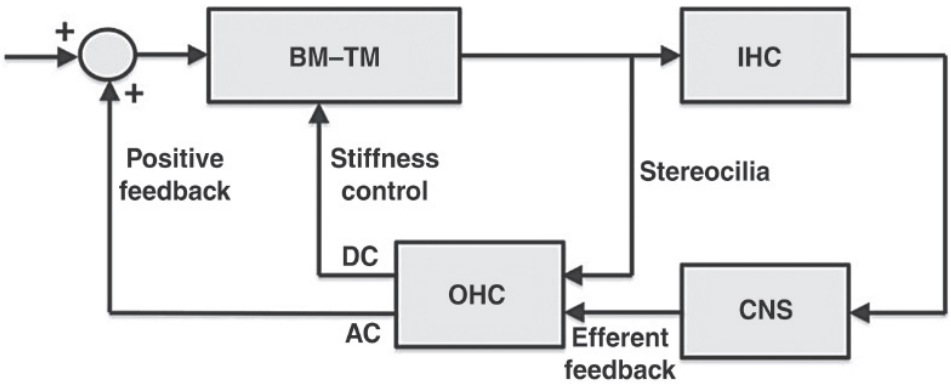

FIGURE 5.23 Black-box control scheme to summarize the relevant functional elements of the active cochlear partition. It includes a DC parametric stiffness regulation, as well as cycle-to-cycle AC positive feedback from the OHCs to BM at the acoustic frequency. The OHCs in turn are controlled by an efferent feedback signal from the CNS that saturates their electro-motility response at high sound levels. The passive properties of the cochlea are provided by the hydrodynamic interactions with BM–TM.

Dallos and Evans, 1995; Ashmore 2008], or, instead, is due to active compression of the BM response (adding damping, eg, Van der Heijden, 2014). In other words: do OHCs provide precise in-phase high-frequency positive feedback to the BM, or do they stiffen to attenuate the BM response at high intensities? In vivo recordings of OHC motion at high frequencies are needed to settle this important issue (Ashmore et al., 2010).

A critical nonlinear oscillator? Taken together, four nonlinear cochlear phenomena underlie the function of the inner ear: (1) a high amplification increases the sensitivity of the system at low sound levels; (2) frequency selectivity increases the spectral resolution of the system; (3) a compressive nonlinearity strongly increases the dynamic range for sound input pressure levels. According to Hudspeth and coworkers, all three phenomena can be captured by a single nonlinear mechanism: a critical oscillator that is tuned to operate closely to a so-called Hopf bifurcation; (4) As an epiphenomenon of this critical system, spontaneous oscillations may occur, which are indeed recorded as spontaneous oto-acoustic emissions (OAEs) by the mammalian (and nonmammalian) ear. Interestingly, the dependence of the nonlinear distortion products of so-called evoked OAEs on the intensities of pairs of input tones is explained by the same Hopf mechanism (Camalet et al., 2000; see also Reichenbach et al., 2012 for an additional hydrodynamic mechanism that mediates the wave propagation of nonlinear distortion products like $2f_1 - f_2$ frequency components towards the middle ear along Reissner's membrane).

A Hopf bifurcation can occur in a dynamical system that has a cubic nonlinearity and is described by the following generic form:

$$\frac{dz}{dt} = z\left(\lambda + i + b|z|^2\right) \qquad (5.62)$$

$$\text{with} \quad [z = x + iy,\ b = \alpha + i\beta] \in \mathbb{C}, \quad \text{and} \quad \lambda \in \mathcal{R}$$

The parameter λ is a control variable that tunes the behavior of $z(t)$. If $\lambda > 0$, and $\alpha < 0$ the system's solution attains a stable limit cycle (called supercritical oscillation), which is described by:

$$z_{LIM}(t) = \sqrt{\frac{\lambda}{|\alpha|}} e^{i\left(1+\beta r^2\right)t} = re^{i\omega_0 t} \tag{5.63}$$

When this nonlinear system is near the critical bifurcation point at $\lambda = 0$, and is driven by an oscillatory stimulus at its characteristic frequency:

$$f(t) = F\exp\left(i\omega_0 t\right) \tag{5.64}$$

so that

$$\frac{dz}{dt} = z\left(\lambda + i + b|z|^2\right) + f(t) \tag{5.65}$$

the response amplitude varies with stimulus amplitude, F, through a compressive power law relation:

$$|z| \propto F^{1/3} \tag{5.66}$$

This compressive nonlinearity nicely corresponds to the amplitude-dependent gain of the cochlear amplifier seen in the recordings of Fig. 5.17: a high gain for low-intensity sounds, and a low gain for high-intensity sounds, as the gain is defined by (Fig. 5.24):

$$G = \frac{d|z|}{dF} \propto \frac{1}{F^{2/3}} \tag{5.67}$$

Note that the discrete nonlinear feedback model of Nobili et al. (1998), described by Eq. (5.59), can be rewritten such that the OHC nonlinearity, OHC(z_n), in their model contains the cubic nonlinear term that is required for the Hopf bifurcation in Eq. (5.62) (Hudspeth et al., 2010).

5.5 EXERCISES

Problem 5.1:

(a) Show that Eq. (5.12) is indeed a solution that obeys the dry-water constraints Eqs. (5.9, 5.10).
(b) Make the deep-water wave approximation to show Eq. (5.13).
(c) Same for the shallow-water wave approximation of Eq. (5.14).

Problem 5.2:

(a) Derive the dispersion relation for gravitational water waves, Eq.(5.17).

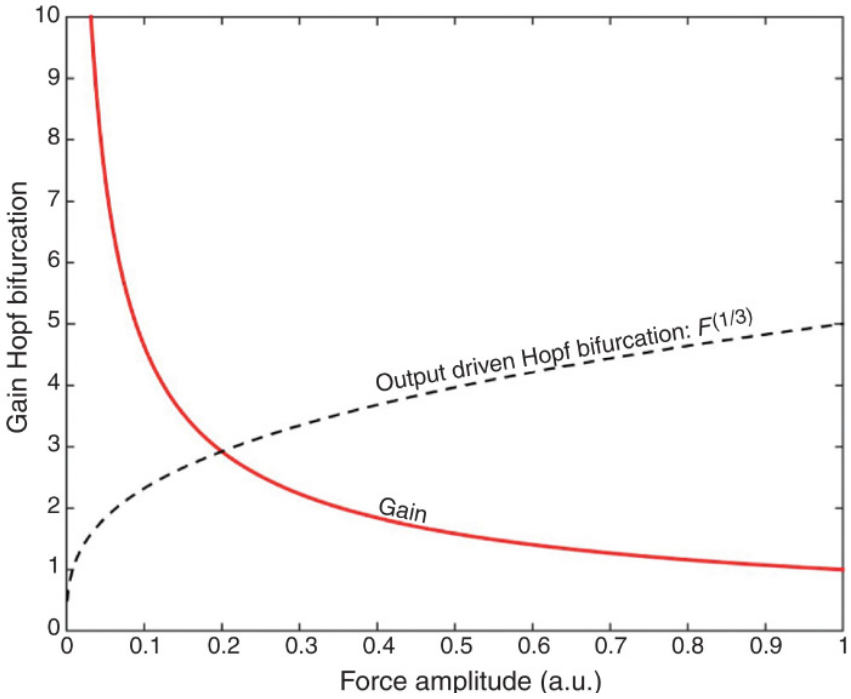

FIGURE 5.24 **Response gain (*red line*) and output (*dashed line*) of the driven Hopf bifurcation, as described by Eqs. (5.66 and 5.67).**

(b) Compute the phase velocity for deep-water waves. What is the group velocity?
(c) The same for shallow-water waves.

Problem 5.3:

(a) Apply the combined effects of gravity and tension to determine the total dispersion relation of dry water, Eq. (5.21).
(b) Determine the phase- and group velocity.
(c) Show that there is one particular wave length, for which phase- and group velocities are identical (which wave length? How high is this velocity?).

Problem 5.4: Consider an infinite basin of dry water, stretching from $x \in [-\infty,+\infty]$. Ignore the z-dimension. For $x < 0$ the depth of the basin is $h = h_1$, so that $y_{\text{bottom}} = -h_1$. At $x = 0$, the bottom profile suddenly jumps upward to $h = h_2 < h_1$. A traveling water wave comes from the left ($x < 0$) at amplitude A, and moves rightward. We consider the deep-water case, that is, $\lambda \ll h_{1,2}$.

(a) Compute the reflection, R, and transmission, T, at $x = 0$ (use: *impedance*).
(b) Same for the shallow-water case, $\lambda \gg h_{1,2}$.

Problem 5.5: Negative dynamic feedback with a delay can cause instability problems. In this Exercise we analyze the influence of a delay on the transfer characteristic of a linear system with feedback (Figs. 5.25 and 5.26).

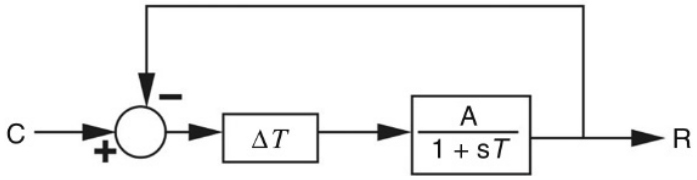

FIGURE 5.25 **Dynamic feedback model of a low-pass filter with a delay.**

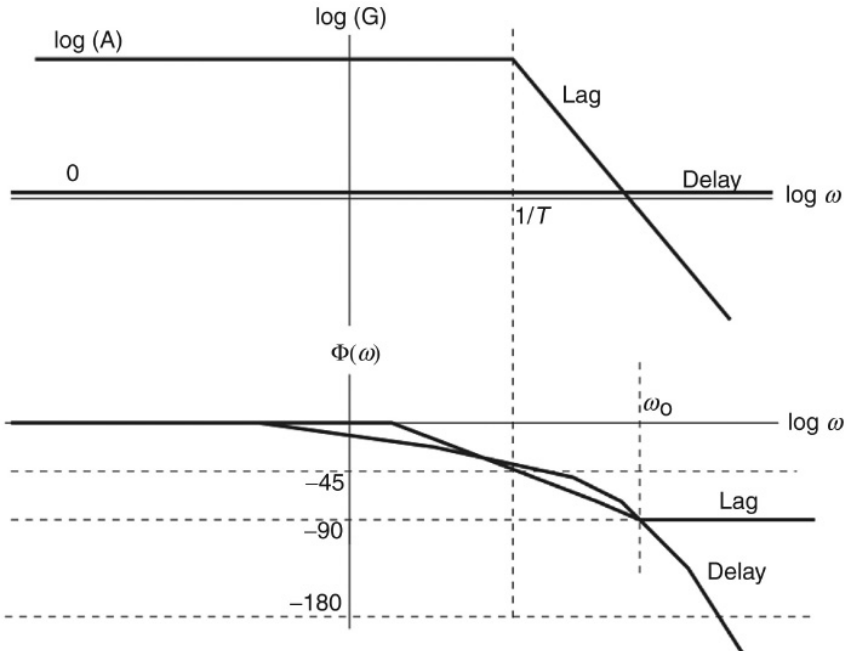

FIGURE 5.26 **Bode plot for the two subsystems.**

(a) Determine the Laplace transform of a pure delay: $y(t) = x(t - \Delta T)$, and from that calculate its transfer characteristic in the frequency domain.

(b) Consider the system shown in Fig. 5.25. Determine the total transfer function and the loop gain. The system will spontaneously oscillate, and thus become unstable, when the loop-gain exceeds the value of 1, and at the same time has a phase shift of −180 degrees. Perform a Bode analysis on this system and estimate the frequency $\omega 0$ where instability kicks in (Fig. 5.26).

(c) What happens to the system if A is increased/lowered? What if the time constant T is increased/lowered?

Problem 5.6: The wave equation of the BM as deduced by Von Békésy and Zwislocki is linear, which means that the superposition principle should hold, and that the output amplitude of the BM is independent of stimulus amplitude. However, when you listen (carefully) to a superposition of two frequencies, say $f_1 = 440$ Hz (musical "A") and $f_2 = 523$ Hz (musical "C"), you can hear the presence of a third tone with a frequency that is close to the musical "F" (349 Hz)! This additional tone is a *combination tone*, and tends to have a frequency of $2f_1 - f_2 = 357$ Hz. This combination tone is a manifestation of a nonlinearity in

the system, and is due to the nonlinear cochlea (note that the effect disappears when the two tones are presented to different ears!).

Suppose, for simplicity, that the output of the BM, $q(t)$, depends on the instantaneous pressure, $p(t)$, through the following nonlinear third-order relation (a third-order Taylor approximation on the nonlinear transfer function):

$$q(t) = ap(t) + bp^2(t) + cp^3(t) \tag{5.68}$$

(a) By presenting a superposition of two harmonic waves at the input, say

$$p(t) = \cos(\omega_1 t) + \cos(\omega_2 t)$$

show that the output of the system can described by a spectrum that contains 13 frequencies! Determine also their relative amplitudes. Which nonlinear term causes the observed "F" percept?

(b) What happens to the amplitude(s) of the distortion products if the input is given by $p(t) = A\cos(\omega_1 t)$

Problem 5.7: Analysis of a Hopf bifurcation. Consider the Hopf bifurcation in polar coordinates (with a and μ nonzero real-valued parameters):

$$\begin{aligned} \frac{dr}{dt} &= r\left(a - \mu r^2\right) \\ \frac{d\phi}{dt} &= \omega_0 \end{aligned} \tag{5.69}$$

Investigate the stability of the fixed points as function of the parameters. When do we see a limit cycle? What determines its amplitude and frequency?

REFERENCES

Ashmore, J., 2008. Cochlear outer hair cell motility. Physiol. Rev. 88, 173–210.

Ashmore, J., Avan, P., Brownell, W.E., Dallos, P., et al., 2010. The remarkable cochlear amplifier. Hear. Res. 266, 1–17.

Brendin, L., Flock, A., Canlon, B., 1989. Sound-induced motility of isolated cochlear outer hair cells is frequency-specific. Nature 342, 814–816.

Camalet, S., Duke, T., Jülicher, F., Prost, J., 2000. Auditory sensitivity provided by self-tuned critical oscillations of hair cells. Proc. Natl. Acad. Sci. USA 97, 3183–3188.

Crawford, Jr., F., 1968. Berkeley physics course. Waves, vol. 3, McGraw-Hill, New York.

Dallos, P., 1973. The Auditory Periphery. Biophysics and Physiology. Academic Press, New York.

Dallos, P., 1992. The active cochlea. J.Neurosci. 12, 4575–4585.

Dallos, P., Evans, B.N., 1995. High-frequency motility of outer hair cells and the cochlear amplifier. Science 267, 2006–2009.

Dannhof, B.J., Roth, B., Bruns, V., 1991. Length of hair cells as a measure of frequency representation in the mammalian inner ear? Naturwissenschaften 78, 570–573.

Fettiplace, R., Hackney, C., 2006. The sensory and motor roles of auditory hair cells. Nat. Rev. Neurosci. 7, 19–29.

Hudspeth, A.J., 1985. The cellular basis of hearing: the biophysics of hair cells. Science 230, 745–752.

Hudspeth, A.J., 2014. Integrating the active process of hair cells with cochlear function. Nat. Rev. Neurosci. 15, 600–614.

Hudspeth, A.J., Jülicher, F., Martin, P., 2010. A critique of the critical cochlea: Hopf – a bifurcation – is better than none. J. Neurophysiol. 104, 1219–1229.

Johnstone, B.M., Boyle, A.J.T., 1967. Basilar membrane vibration examined with the Mössbauer technique. Science 158, 389–390.

Johnstone, B.M., Patuzzi, R., Yates, G.K., 1986. Basilar membrane measurements and the travelling wave. Hearing Res. 22, 147–153.

Nobili, R., Mammano, F., Ashmore, J., 1998. How well do we understand the cochlea? Trends Neurosci. 21, 159–167.

Reichenbach, T., Stefanovic, A., Nin, F., Hudspeth, A.J., 2012. Waves on Reissner's membrane: a mechanism for the propagation of otoacoustic emissions from the cochlea. Cell Reports 1, 374–384.

Russell, I.J., Legan, P.K., Lukashkina, V.A., Lukashkin, A.N., Goodyear, R.J., Richardson, G.P., 2007. Sharpened cochlear tuning in a mouse with a genetically modified tectorial membrane. Nat. Neurosci. 10, 215–223.

Scherer, M.P., Gummer, A.W., 2004. Vibration pattern of the organ of Corti up to 50 kHz: evidence for resonant electromechanical force. Proc. Natl. Acad. Sci. USA 101, 17652–17657.

Van der Heijden, M., 2014. Frequency selectivity without resonance in a fluid waveguide. Proc. Natl. Acad. Sci. USA 111, 14548–14552.

Zwislocki, J.J., Kletsky, E.J., 1979. Tectorial membrane: a possible effect on frequency analysis in the cochlea. Science 204, 639–641.